SAPIENZA
UNIVERSITÀ DI ROMA

Facoltà di Ingegneria

TESI DI LAUREA MAGISTRALE IN

INGEGNERIA DELLE COMUNICAZIONI

Impact of Time Reversal on Multi-User Interference In UWB-IR Communication Systems

Candidato:
Guido Capodanno
Matr. 1086638

Relatore:
Prof.ssa Maria-Gabriella Di Benedetto

Correlatore:
Prof. Jocelyn Fiorina

Anno Accademico 2009/2010

A mia madre,

il cui amore è incrollabile certezza.

A mio padre,

irraggiungibile modello di saggezza.

Contents

List of Figures

List of Tables

Chapter 1

Introduction

"Life would be infinitely happier if we could only be born at the age of eighty and gradually approach eighteen." (M. Twain)

The aim of this work, developed in Supélec (Ecole supérieure d'électricité, Plateau de Moulon, Gif-sur-Yvette, France) is to show how Time Reversal applied to UWB-IR systems has an impact on Multi-User Interference (MUI) distribution, that changes compared to traditional case. We will show the limitiations in modeling the MUI distribution as a Standard Gaussian and that the use of Time Reversal, in a UWB-IR communication system affected by multi-user interference, leads to improved performance both with a classical rake receiver and with a receiver adapted to a Generalized Gaussian distribution, that fits MUI distribution better than the Standard Gaussian in those UWB-IR systems that make use of Time Reversal.

In the detail, the following chapters are organized as follows. After this introduction, in **Chapter 2** a general overview on Ultra Wide Band - Impulse Radio communication systems is presented. After the brief introduction to UWB signals, reference transmitters and receivers, we talk about MUI,

underlining the limitations of SGA in describing the real performances of correlation receiver [5] and the fact that SGA could be a valid approximation only under particular asymptotic conditions [11]. After the brief introduction to UWB communication systems and UWB-IR signals properties, in **Chapter 3** we describe the Time Reversal (TR) technique, with an overview on its history and the state of the art about its applications, with a particolar focus on its use in UWB-IR systems. In **Chapter 4** we present our study about Time Reversal impact on Multi-User Interference. We will show that Time Reversal, applied to UWB-IR systems, changes the distribution of MUI, that results increasingly tight compared with a Gaussian one if TR impact grows. The study has been conducted in MATLAB, in several reference scenarios with multipath channels, varying transmission parameters (number of users, power transmitted by intended and interfering transmitters, repetition code) and network topologies. We will underline the limits of validity of Standard Gaussian Approximation for the MUI distribution and that the use of Time Reversal, in a UWB-IR communication system affected by multi-user interference, leads to improved performance both with a classical rake receiver and with a receiver adapted to a Generalized Gaussian distribution. The study has been performed in several cases in which the TR technique has been used in a more or less deep way. In **Chapter 5** we summarize the results obtained in this work.

Chapter 2

Overview on UWB-IR Communication Systems

Ultra Wide Band - Impulse Radio (UWB-IR) signals use an impulsive carrier, very short in time, cadenced by a clock. UWB signals have a very large spectral occupation because of the very bandwide nature of the signal, that is not sinusoidal but impulsive, so the power spreads on such a wide band that allows UWB waveforms to overlay over other systems. Therefore, this technology is able to offer low emissions and due to their low spectral density UWB signals can coexist in the radio world, are flexible in providing wireless access to heterogeneous applications, robust to interference. In addiction, they allow high-precision ranging (they are used in the military, radar fields): to integrate positioning and ranging with communication is a very interesting aspect of UWB transmissions. In the last years a great effort has been made in order to reduce the duration of these pulses: this technique goes under the name of "impulse radio". In order to verify the possibility for UWB systems to coexist with other existing systems, several measurement campaigns were performed in the United States by research institutes

and agencies, with the result that in 2002 FCC allowed UWB transmissions complying with outdoor and indoor emission masks: the band that the FCC allocated to communications is 7.5 GHz between 3.1 and 10.6 GHz and the maximum EIRP emission level has to be less than the part 15 (limit for maximum involuntary emissions). According to FCC, a signal is UWB if it has a

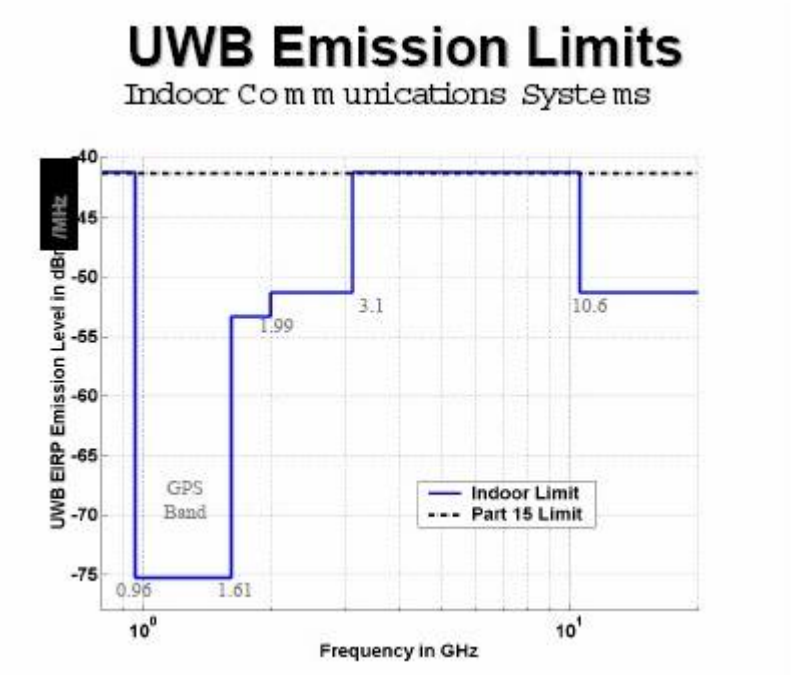

Fig. 2.1: FCC emission mask for indoor communications.

center frequency less than 2.5 GHz and Fractional Bandwtih ¿0.20 or center frequency greater than 2.5 GHz and bandwith greater than 500 MHz. The Fractional Bandwith is defined as follows:

$$FB = \frac{f_h - f_l}{\frac{f_h + f_l}{2}}$$

where f_l and f_h are set to the lower and upper frequencies of the -10 dB emission points. An high fractional bandwith is obtained with very short impulses, charachterized by a duration of hundreds of picoseconds, without

RF modulation. The general tx/rx chain for a multi-user system that uses the UWB technology is shown in Fig. 2.2

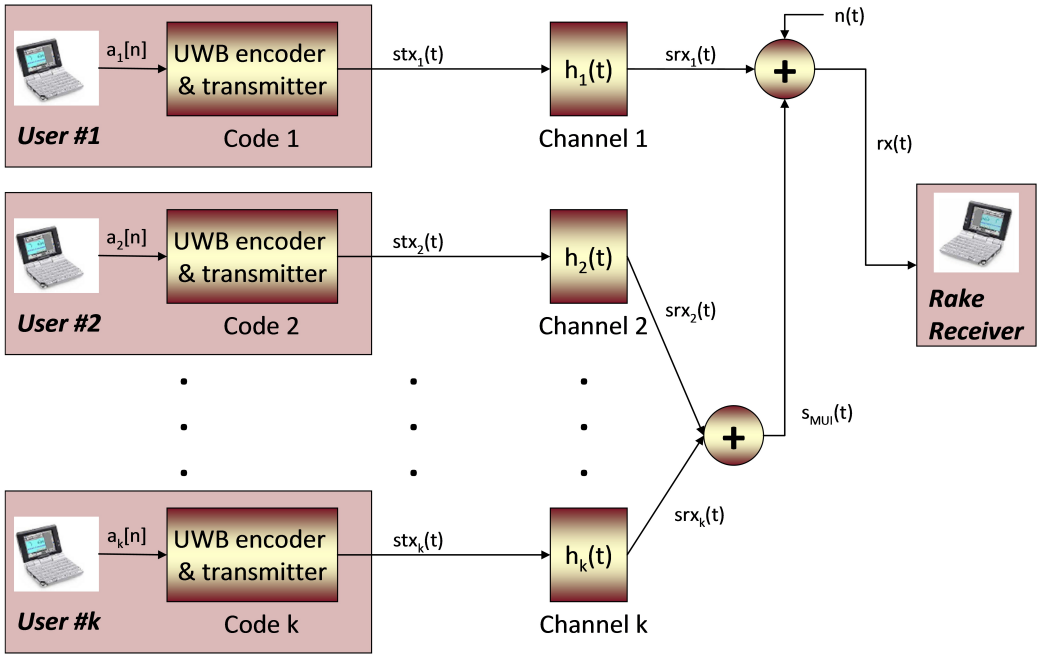

Fig. 2.2: General tx/rx scheme for an UWB system

2.1 UWB encoder and transmitter

The most common way of generating an UWB signal is by emitting very short pulses, with a duration of few hundreds picoseconds. It is remarkable that, because of the short duration of pulses, there is no need of RF mixing stage, so impulse radio has the significant advantage of being essentially a baseband technique (the UWB signal spans frequencies commonly used as carrier frequencies) and this simplify the transmitter/receiver structure. In order to modulate the signal with the information data, we can play with pulse position or amplitude, obtaining a Pulse Position Modulation

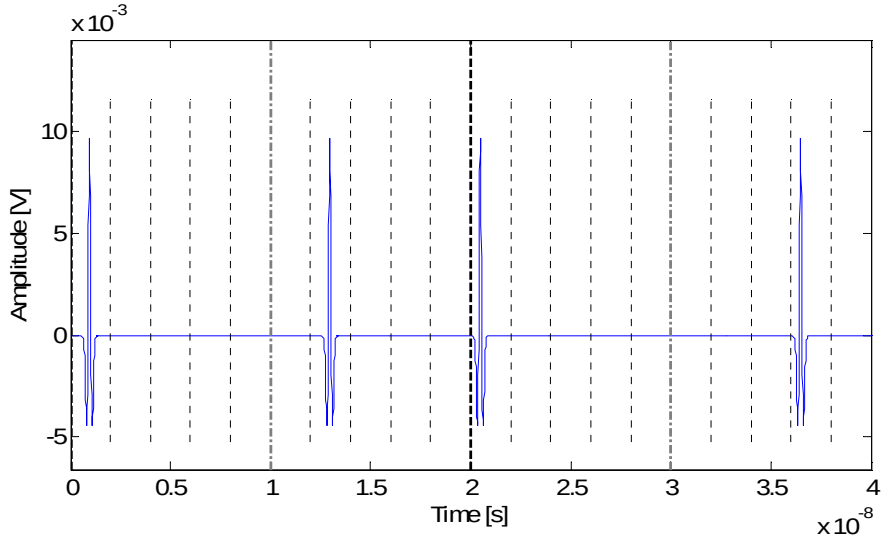

Fig. 2.3: 2PPM-TH-UWB signal; bits=[1 0]; THCode=[0 1 0 3]; ϵ =0.5 ns; $N_s = 2$; $T_c = 2$ ns (chip time); $T_s = 10$ ns (pulse period).

(PPM) or a Pulse Amplitude Modulation (PAM), encoding data symbols using pseudo-noise (PN) codes to avoid collisions in multiple access. We could also introduce a repetition code, using N_s pulses for the transmission of the same information bit. An example of binary pulse position modulated UWB signal with Time Hopping code (2PPM-TH-UWB) is shown in Fig. 2.3. We can also consider a binary pulse amplitude modulation with a direct sequence code (2PAM-DS-UWB). An example of 2PAM-DS-UWB signal is shown in Fig. 2.4. The binary PAM (2PAM) modulation leads to a greater intersymbol distance with respect to binary PPM (2PPM), that needs 3 dB more than 2PAM to achieve the same Bit Error Rate. However, if we increase the number of levels from 2 to m, the performances of a system that use a mPPM scheme are better than mPAM. In addiction, the PPM produces only one pulse polarity, so the receiver structure can be simpler. In this work, the pulse shape is modelled as the second derivative of a Gaussian function: it

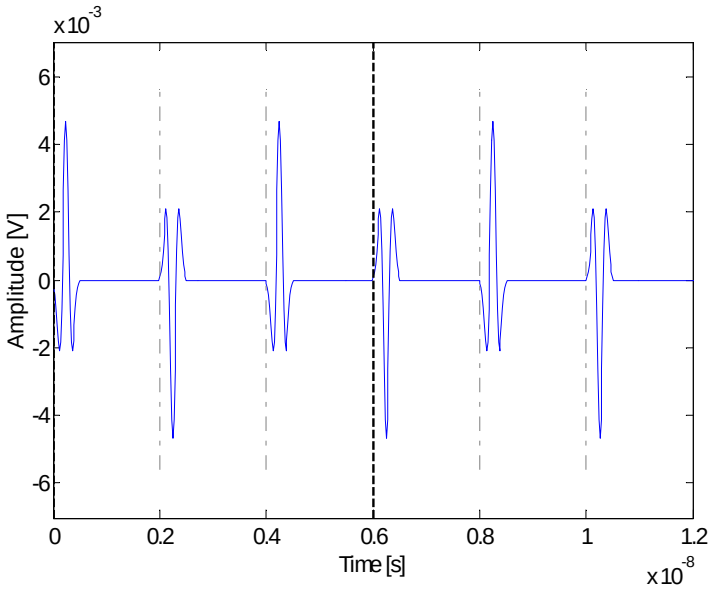

Fig. 2.4: 2PAM-DS-UWB signal; bits= [1 0]; DSCode=[1 -1 1]; $N_s = 3$.

approximates quite well what is sent in air, which is not perfectly symmetric. In addiction, it is less expensive to generate non-sinusoidal pulses than pulse-modulated sinewaves. The analytical expression of a gaussian pulse is as follows:

$$p(t) = \pm \frac{1}{\sqrt{2\pi\sigma^2}} e^{-\frac{t^2}{2\sigma^2}} = \pm \frac{\sqrt{2}}{\alpha} e^{-\frac{2\pi t^2}{\alpha^2}}$$

Where $\alpha^2 = 4\pi\sigma^2$ is the shape factor and σ^2 is the variance.

2.2 Ultra Wide Band receivers

In wireless channels, a signal may go through different fading paths having different lengths and the signals travel at the same speed, but the signal arrival times for the paths differ. Due to reflections from obstacles a radio channel can consist of many copies of originally transmitted signals having different amplitudes, phases, and delays. In addiction, UWB signals have an

ultra wide bandwith occupation, leading to a very multipath rich channel but to an enhanced resolution power of the system, with an high capacity to distinguish between multipath replicas if we use a diversity reception technique like the Rake Receiver. Multipath can occur in radio channel in various ways, such as reflection, diffraction, scattering. The channel models proposed by IEEE and considered in this work will be discussed in the following chapters. Referred to as Impulse Radio, IR-UWB technology offers the possibility of developing high data-rate, low power-consumption communication systems that provide greater immunity to multi-path fading due to the pulse's fine delay resolution [16], and greater Bit-Error Rate (BER) performance at a given Signal-to-Noise Ratio (SNR) due to the signal spreading in spectrum [18]. In order to improve receiver performances in presence of multipath channels, Rake Receiver has been used. It is a diversity technique, widely used in WCDMA systems, that rakes the energy from the multipath propagated signal components, allowing to increase the received energy combining different replicas of the signal, corresponding to different paths. The Rake receiver, in fact, consists of "fingers", each of them corresponding to one path delay of a received signal and utilizes multiple correlators to separately detect the multipath components. Obviously, rake receiver has to know:

- multipath delays $\rightarrow$ time delay synchronization;
- amplitudes of the multipath components $\rightarrow$ amplitude tracking;
- number of multipath components $\rightarrow$ RAKE allocation.

Therefore, channel estimation alghoritms must be used to get these information on the channel. Numerous approaches to channel estimation in UWB communication systems have been suggested, but there are significant drawbacks associated with HW implementation of each of them. In general, these

issues regard the sampling frequency and are an inherent aspect of UWB, given that the spectrum allocated for such signals is from 3.1 GHz to 10.6 GHz. To sample at or above the Nyquist rate becomes problematic in a physical device given the large bandwidth of the UWB signals themselves. An example of reduced complexity RAKE receiver that still utilizes correlator outputs before combining them for the symbol decision, but without the use of channel estimation has been proposed by [22]. The main challenges for RAKE receivers operating in multipath channels are in receiver synchronization. For our purposes, we have assumed a time delay synchronization between the reference transmitter and the receiver. As we said, RAKE receiver attempts to collect the time-shifted versions of the original signal by providing a separate correlation for each of the multipath componentes associated to a signal, comibining their energies before decision. This implies a remarkable complexity in the receiver, that in the ideal case has to consist of a bank of parallel N correlators, where N is the number of all different paths: in this case, we have an All-rake or "A-RAKE" receiver. A pratical implementation of a rake receiver uses only the S best propagation paths (Selective rake or "S-RAKE"), leading to worse performances with respect to A-RAKE but to a simpler receiver structure. Another possibility is to use the first L multipath components: in this case we have a Partial rake or "P-RAKE". Note that S-RAKE differs from P-RAKE because the strongest components are not necessarly the first ones. In this work, we have used S-RAKE and A-RAKE (receiver side) in combination with Time Reversal (transmitter side). The S-RAKE structure is shown in Fig. 2.5. L is the number of correlators, which are called Rake fingers, $m_i(t)$ is the correlation mask of finger i, ω_i denotes the weighted parameter according to the receiver scheme. Examples of S-RAKE receivers correlator masks for 2PPM-UWB

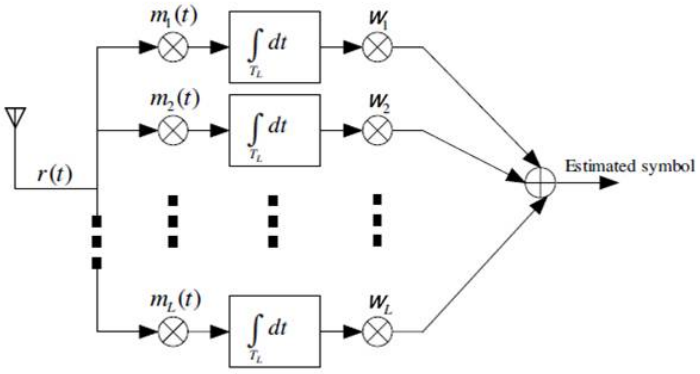

Fig. 2.5: S-RAKE receiver structure

signals in presence of the channel shown in Fig. 2.6, with a reference pulse in Fig. 2.7, are shown in Fig. 2.8, Fig. 2.9, Fig. 2.10.

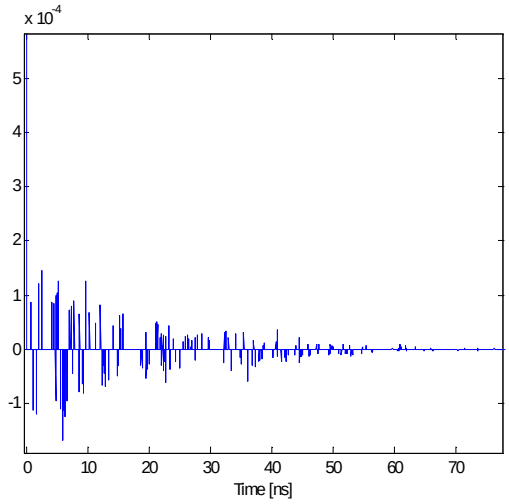

Fig. 2.6: Example of IEEE 802.15.3a multipath channel

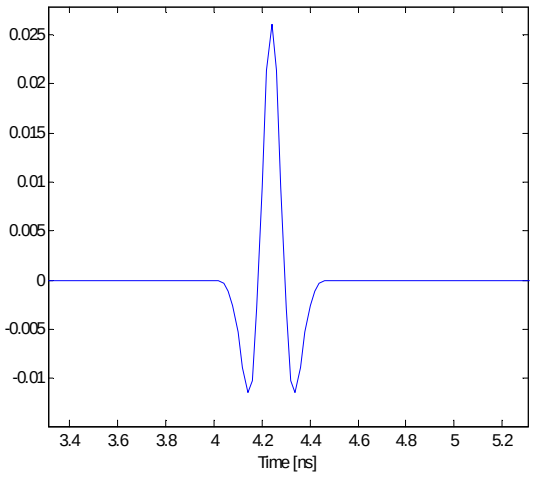

Fig. 2.7: Reference pulse transmitted through the channel

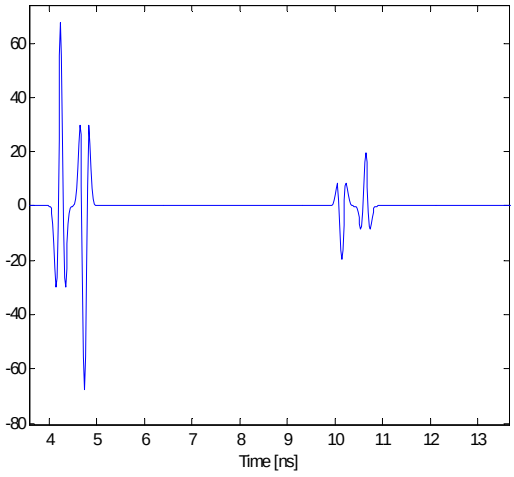

Fig. 2.8: S-RAKE receiver mask for 2PPM-UWB signal with 2 fingers

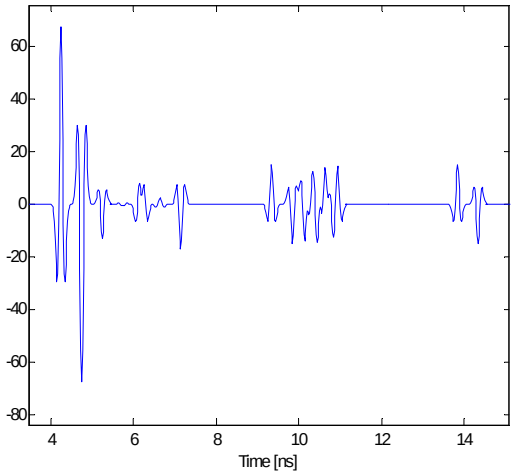

Fig. 2.9: S-RAKE receiver mask for 2PPM-UWB signal with 10 fingers

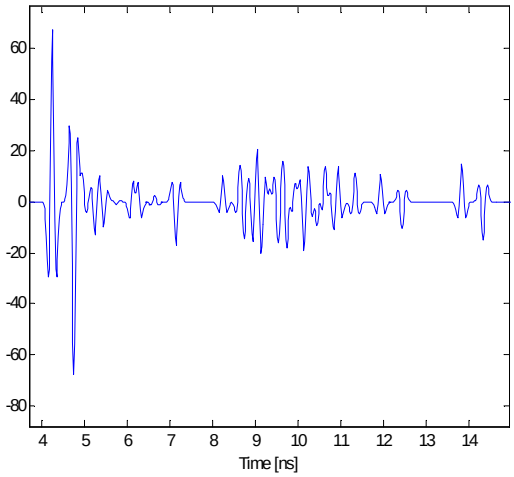

Fig. 2.10: S-RAKE receiver mask for 2PPM-UWB signal 20 fingers

2.3 Multi User Interference in UWB systems

The Multi User Interference (MUI) is one of the most important elements that generally limits the performances of the correlation receiver, a receiver known for its low complexity and for its ability to collect multipath diversity. For simplicity, a SGA (Standard Gaussian Approximation) on MUI is often assumed: MUI is modelled as a Gaussian random process, just like thermal noise. In UWB systems, this approximation leads to theoretical results in contradiction with ones obtained by the simulations, with an optimistic estimate of BER vs. SNR. For instance, we can refer to Durisi and Romano. In their work, the authors assumed a gaussian model for multi-user interference in the case of TH binary PPM modulation scheme, they derived an analytical expression for BER and then they compared the theoretical results with ones derived from simulations. Referring to the general tx/rx scheme of Fig. 2.2, when Nu users are active, if we consider only AWGN neglecting for the moment the multipath channels, then the received signal can be modelled in the following way [5]:

$$r(t) = \sum_{k=1}^{Nu} A_k s_{rx}^{(k)}(t - \tau_k) + n(t) = A s_{rx}^{(1)}(t - \tau_1) + \sum_{k=2}^{Nu} A_k s_{rx}^{(k)}(t - \tau_k) + n(t)$$

where A_k and τ_k, for $k = 1, \ldots, Nu$ are the attenuations over the channel and the time delays associated to propagation and asynchronism between the users, respectively. In order to analitically evaluate the effect of MUI, the following assumptions are made:

1. The elements $c_j^{(k)}$ of the Time Hopping code for $k = 1, \ldots, Nu$ and for all j are independent identically distributed (i.i.d.) discrete random variables, uniformly distributed on the interval $[0, N_h)$.

2. Time delays τ_k are i.i.d. random variables, with:

$$\alpha_{1,k} = (\tau_1 - \tau_k) mod(T_f - \frac{T_f}{2})$$

uniformly distributed on $(-\frac{T_f}{2}, \frac{T_f}{2})$, for $k = 1, \ldots, Nu$.

3. The signals $s_{rx}^{(k)}(t - \tau_k)$ and noise $n(t)$ are all assumed to be independently generated.

4. Time Hopping is allowed only on the first half of the frame interval, i.e. $N_h T_c \leq \frac{T_f}{2}$.

According to SGA, the overall interference:

$$n_{tot}(t) = \sum_{k=2}^{Nu} A_k s_{rx}^{(k)}(t - \tau_k) + n(t)$$

is assumed to be a zero mean gaussian random process. In their study, the authors show the extremely limited capacity of SGA to describe the real performances, especially when $T_c > T_M$, being T_M the wave duration. Comparison between theoretical analysis and simulation shows the non validity of Gaussian model to characterize the multi user interference in TH binary PPM systems. In particular, the BER floor is different with the two approaches and the gaussian model results in a more optimistic prediction. In **Chapter 4** we will verify that this aspect is more marked in a UWB-IR system that makes use of TR.

Even if the SGA shows several limitations in describing the real performances of the correlation receiver, the Gaussian property simplifies performance calculation, and furthermore, Gaussian noises are well handled by a large number of forward-error coding and decoding techniques. From a probabilistic point of view, the Gaussian approximation can be justified naturally by a Central Limit Theorem (CLT) argument. To obtain a CLT, one has to

define an asymptotic regime where the number of interfering users grows to infinity while the contribution of every interferer to the total MUI becomes infinitesimal [13]. In order to justify the assumption of modeling MUI at the output of correlation receiver as a Gaussian random variable, the conditions of validity of the Central Limit Theorem (CLT) have been studied by Fiorina et al., in the asymptotic regime where the number of interferers and the spreading factor grow toward infnity at the same rate. Non synchronized users sending their signals over independent multi-path channels and having possibly different powers have been considered by the authors. It has been shown that, both for the TH-PAM and the TH-PPM case, when the frame length grows and the repetition factors kept constant, then the MUI does not converge in distribution toward a Gaussian random variable. On the other hand, this convergence can be established if the repetition factor grows at the rate of the frame length. The asymptotic regime has been characterized beginning with frequency occupation considerations. The effective pulsewidth is denoted by T_M and the duration of a time slot by $T_{c]}$, the usually so-called chip time interval. The frequency band of an UWB signal is of the order of $1/T_M$, and the data symbol rate is equal to $1/N_s N_h T_c$. As a spread-spectrum system, the UWB system will then have a processing gain of $N_s N_h T_c/T_M$. Ignoring the factor T_c/T_M, the authors call *processinggain* the integer $N = N_s N_h$. Denoting by K the number of users supported by the system, the total number of symbols per second carried by the UWB signal is equal to $K/(N_s N_h T_c)$. In these conditions, it is reasonable to consider the ratio of the number of transmitted symbols per second to the system bandwidth KT_M/NT_c as a system load. Dropping again the factor T_M/T_c, load is assumed K/N. In this case, the asymptotic regime is then characterized by the fact that $N \to \infty$ and the number of users $K \to \infty$ in such a way

that K/N converges toward a constant $\alpha > 0$; in other words, the number of contributors grow, thus permitting to consider CLT results, but the number of symbols per second per Hertz transmitted by the whole system is constant. This general point of view is often adopted in asymptotic studies for direct-sequence CDMA (DS-CDMA) systems. The result is that when $N_h \to \infty$ and N_s is kept constant, the MUI term r_{MUI}, associated to the variable at the output of the correlator when in input there is the MUI signal, does not converge in distribution to a Gaussian random variable. On the other hand, it does if $N \to \infty$, $N_s/N_h \to \rho > 0$ and $K/N \to \alpha$. Fig. 2.11 shows the histograms of the variable r_{MUI} in the case of TH-PAM transmission with power control. The centered Gaussian densities with variances $E[r_{MUI}]^2$ are also shown in the figure. From the top to the bottom of Fig. 2.11, K and N increase in such a way that the load α is fixed to 1/2. In the left column, N_s is fixed to 1. Here, as predicted, the MUI distribution does not approach the Gaussian distribution as N_h grows. Alternatively, when N_s grows in parallel with N_h (right column), the MUI distribution approaches the Gaussian distribution. Simulations have also been conducted in a more realistic environment, where the channels are multi-path channels and the received powers are different. The histograms of r_{MUI} for this case are shown in Fig. 2.12. In summary, assume that K and N are fixed to large enough values. A too small value of N_s will result in a non-Gaussian MUI distribution, which is, in general, harmful in the sense that the Gaussian approximation predicts a much better BER. It is also to notice that to reach the domain of validity of the asymptotic regime, we have to use a large processing gain and a large number of users. It is clear that at a fixed chip rate, a high processing gain leads to a reduced bit rate per user. Therefore, the asymptotic analysis of the Gaussian approximation is valid in the context of networks with rela-

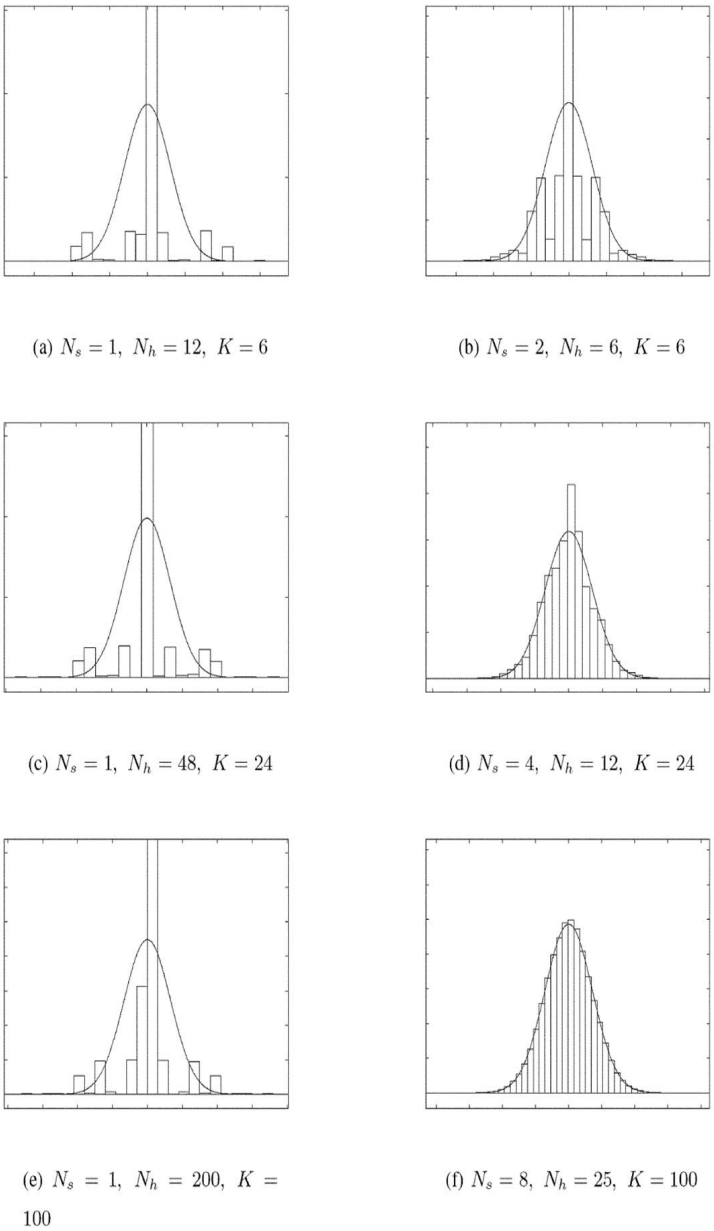

(a) $N_s = 1,\ N_h = 12,\ K = 6$

(b) $N_s = 2,\ N_h = 6,\ K = 6$

(c) $N_s = 1,\ N_h = 48,\ K = 24$

(d) $N_s = 4,\ N_h = 12,\ K = 24$

(e) $N_s = 1,\ N_h = 200,\ K = 100$

(f) $N_s = 8,\ N_h = 25,\ K = 100$

Fig. 2.11: Measured MUI histograms (bars) and reference Gaussian distributions with same variances (plain curves). Single path channels [13].

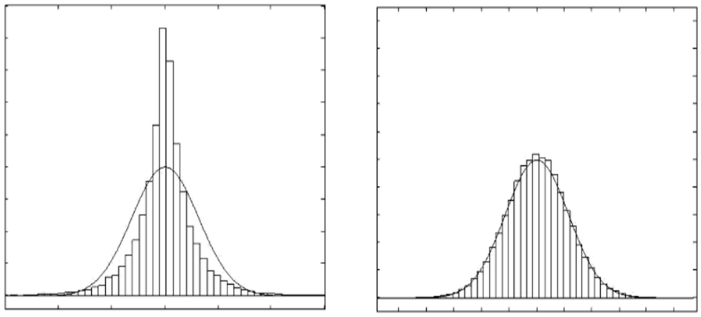

(a) $N_s = 1,\ N_h = 600$ (b) $N_s = 6,\ N_h = 100$

Fig. 2.12: Measured MUI histograms (bars) and reference Gaussian distributions with same variances (plain curves). Multipath channels [13].

tively low rates per user. Therefore, the asymptotic analysis of the Gaussian approximation is valid in the context of networks with relatively low rates per user rather than in the context of high speed WPAN. In these contexts, the asymptotic analysis can be used.

Chapter 3

Time Reversal and its applications to UWB

After the brief introduction to UWB communication systems and UWB-IR signals properties, now we describe the Time Reversal (TR) technique, with an overview on the state of the art about its applications. Then, we will discuss about TR's utilization in UWB-IR communication systems. Because of their features, the UWB signals are very suitable to be used in association with TR, that in the last years has become an interesting topic beacuse it can allow to improve performances in presence of multipath channels and Multi User Interference (MUI).

3.1 What is Time Reversal?

The idea at the basis of TR technique consists in reversing time, a topic historically present in human mind. For instance, Mark Twain said: "life would be infinitely happier if we could only be born at the age of eighty and gradually approach eighteen". Another example is the movie "The Curious

Case of Benjamin Button", in which the protagonist borns with the physical appearance of a seventy-year-old man and "grows younger". In reality, TR is nothing of the kind, but a method that uses backward propagation of waves to focus wave energy onto a specific location in space and time. In order to understand the TR technique, we can refer to the firsts TR communications experiments, where the intended receiver first broadcasts a short pilot pulse, the transmitter estimates the channel impulse response and then sends the time reversed version of it back into the channel. The emitted time reversed waves back propagate in the channel by retracing their paths and focus in space and time at the source, the intended receiver. In a channel with rich scattering, multipathing or multiple scattering is exploited by TR [2] to focus broadband signals tightly in space and time. Spatial focusing means that the spatial profile of the power peaks at the intended receiver and decays rapidly away from the receiver. Temporal focusing means that the equivalent TR channel impulse response at the receiver has a very short effective length. As we will see in the following, we can create the conditions for UWB-IR-TR transmission using prefilters that ideally have an impulse response $h(-t)$, being $h(t)$ the impulse response of the channel [17]. The time reversal method has been successfully used in acoustics and underwater areas for many years: in the following sections some experiments that have been carried out in these fields are shown. Then, we focus on TR applications in UWB.

3.2 Time Reversal experiments in acoustics

Many studies about Time Reversal in acoustics have been conducted by Mathias Fink et al. [9, 8], which developed acoustic Time Reversal Mirror (TRM), made from an array of transmit-receive transducers that respond

linearly and allow the incident acoustic pressure to be sampled. The pressure field is then time-reversed and re-emitted. It is a device able to refocus an incident acoustic field to the position of the original source regardless of the complexity of the propagation medium [9]. TRM's have now been implemented in a variety of physical scenarios from MHz ultrasonics with order centimeter aperture size to hundreds/thousands of Hz in ocean acoustics with order hundred meter aperture size. In such a device, an acoustic source, located inside a lossless medium, radiates a brief transient pulse that propagates and is distorted by the medium. If the acoustic field can be measured on every point of a closed surface surrounding the medium (acoustic retina), and retransmitted through the medium in a time-reversed chronology, then the wave will travel back to its source. The idea of wave equation invariance under a TR operation in a non-dissipative heterogeneous medium gives the basis of time reversal acoustics. Therefore, for every burst of sound $\phi(\mathbf{r}, t)$ diverging from a source and possibly reflected, refracted or scattered by any heterogeneous media, there exists in theory a set of waves $\phi(\mathbf{r}, -t)$ that precisely retraces all of these complex paths and converges in synchrony, at the original source, as if time were going backwards. These basic ingredients and conclusions apply equally well to elastic waves in solid and to electromagnetic fields. Note that it requires both time reversal invariance and spatial reciprocity to reconstruct the time-reversed wave in the whole volume by means of a two dimensional Time Reversal operation.

3.2.1 Time Reversal in complex media

From an experimental point of view a closed TRM consists of a bidimensional piezoelectric transducer array that samples the wavefield over a closed surface (see Fig. 3.1). An array pitch of the order of $\lambda/2$, where λ is the

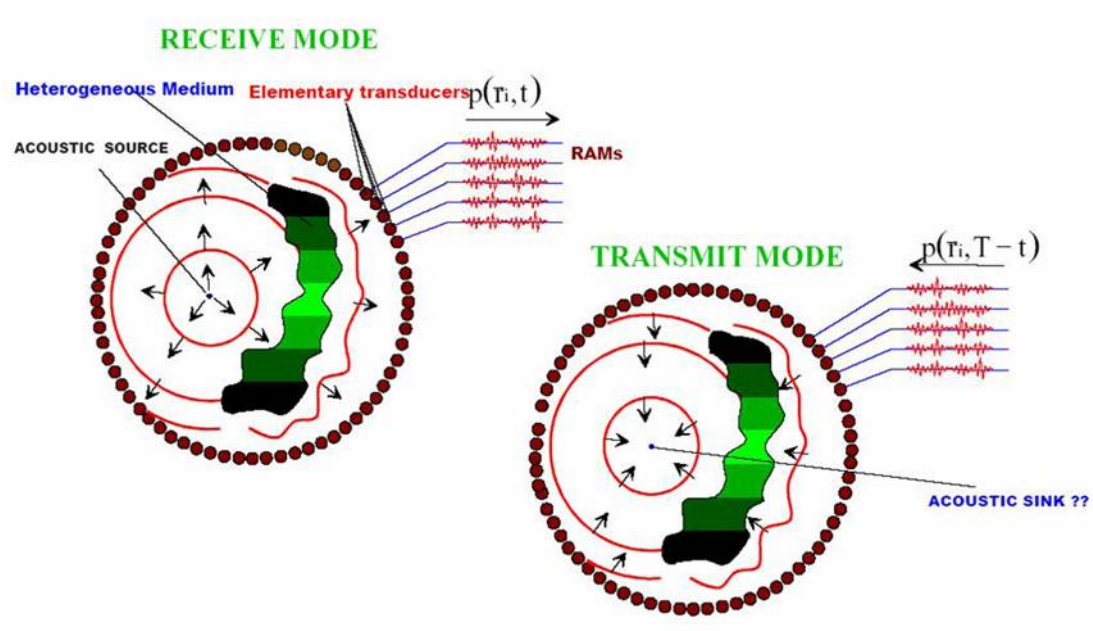

Fig. 3.1: Ideal Time Reversal experiment: (a) Recording step; (b) Time-reversed or reconstruction step. Figure taken from [9].

smallest wavelength of the pressure field, is needed to insure the recording of all the information on the wavefield. Each transducer is connected to its own electronic circuitry that consists of a receiving amplifier, an A/D converter, a storage memory and a programmable transmitter able to synthesize a time-reversed version of the stored signal. In practice, closed TRMs are difficult to realize and the TR operation is usually performed on a limited angular area. This yields an increase of the point spread function dimension that is related to the limited angular size of the mirror observed from the source [9]. In this case, in order to improve focusing quality, we can replace one part of the transducers needed to sample a closed time reversal surface by reflecting boundaries that redirect one part of the incident wave towards the TRM aperture, as shown in Fig. 3.2. In fact, when a source radiates a wave field inside a closed cavity or in a waveguide, multiple reflections along the

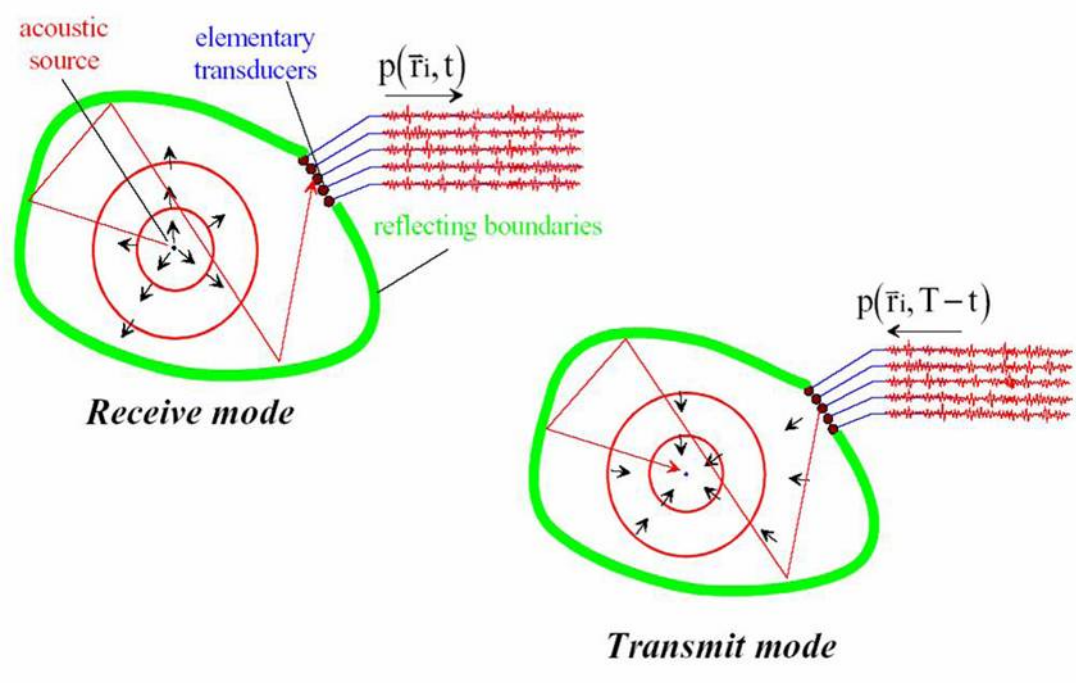

Fig. 3.2: Time Reversal Mirrors in complex media. Figure taken from [9].

medium boundaries can significantly increase the apparent aperture of the TRM ("kaleidoscopic" effect). Thus the spatial information that is usually lost with a finite aperture TRM is converted into the time domain and the reversal quality depends crucially on the duration of the time-reversal window, i.e., the length of the recording to be reversed. A TRM consists typically of a small number of elements or time reversal channels. In the recording step (Fig. 3.1 (a)), a closed surface is filled with transducer elements. A point like source generates a wave front which is distorted by heterogeneities. The distorted pressure field is recorded on the cavity elements. In Time-reversed or reconstruction step (Fig. 3.1 (b)), the recorded signals are time-reversed and reemitted by the cavity elements. The time-reversed pressure field back propagates and refocuses exactly on the initial source. In Fig. 3.2, one part of the transducers is replaced by reflecting boundaries. In the first step (receive

mode) the wave radiated by the source is recorded by a set of transducers through the reverberation inside the cavity. In the second step, the recorded signals are time-reversed and reemitted by the transducers.

3.2.2 Time Reversal in acoustic waveguide

Another experiment that shows how the reflecting boundaries can act as "virtual transducers" has been conducted in the ultrasonic regime by P. Roux et al. [20, 19], that studied this effect with a TRM made of a 1D transducer array located in a rectangular ultrasonic waveguide. The experiments have shown the effectiveness of the TR processing to compensate for multipath effects. For an observer, located in the waveguide, the TRM seems to be escorted by a periodic set of virtual images related to multipath propagation and effective aperture 10 times larger than the real aperture was observed. The experiment was conducted in a waveguide whose interfaces (water air or water-steel interfaces) are plane and parallel. The length of the guide is $L \approx 800$ mm, which is on the order of 20 times the water depth $H \approx 40$ mm. A subwavelength ultrasonic source is located on one side of the waveguide. On the other side, a TRM is used. In total, 96 of the array elements are used, which corresponds to an array aperture equal to the waveguide aperture. All the transducers work around a center frequency of 3.5 MHz with a 50% bandwidth. Due to experimental limitations, the array pitch is equal to 0.7. Then, the experiment is performed in the following way : (1) the point source emits a pulsed wave (1 μs duration), (2) the TRM receives, selects a time reversal window, time-reverses and re-transmits the field which has propagated from the source through the waveguide, (3) after back propagation, the time reversed field is scanned in the plane of the source. Fig. 3.3 shows the incident field recorded by the array after forward

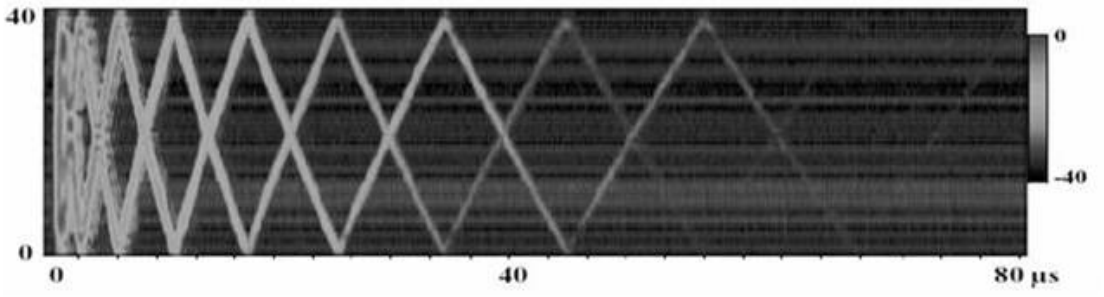

Fig. 3.3: Spatial-temporal representation of the incident acoustic field in acoustic waveguide; the amplitude of the field is in dB [9].

propagation through the channel. After the arrival of the first wavefront corresponding to the direct path we observe a set of signals, due to multiple reflections of the incident wave between the interfaces that spread over 100 μs. Fig. 3.4 represents the signal received on one transducer of the TRM. After the time-reversal of all the signals recorded by the array during 100 μs,

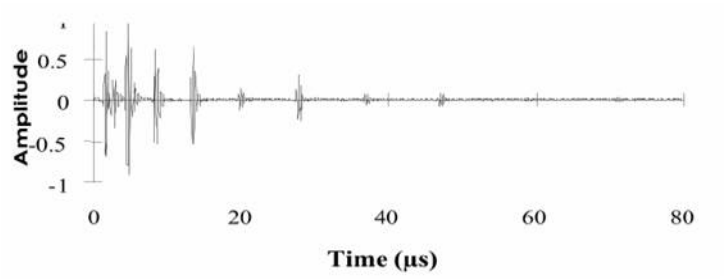

Fig. 3.4: Evolution of the signal measured on one transducer of the array [9].

we observe a remarkable temporal compression at the source location (see Fig. 3.5). This means that multipath effects are fully compensated. The major interest of TRM, compared to classical focusing devices (lenses and beam forming) is certainly the relation between the medium complexity and the size of the focal spot. It must be noticed that the research on time reversal acoustics was initially focused on two main applications: ultrasound

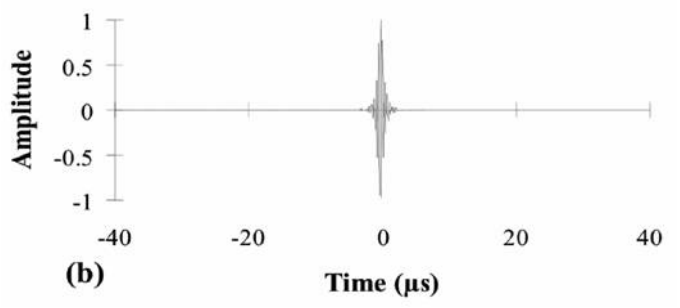

Fig. 3.5: Time-reversed signal measured at the point source [9].

therapy (tumor or kidney stone destruction) and acoustic communications in the ocean. In both applications, self focusing on the source with a TRM is accomplished without any knowledge of the medium between the source and the TRM.

3.2.3 Time Reversal through random media

Some experiments regarding TR with random media placed between the source and an acoustic array (see Fig. 3.6) have been carried out by Derode et al. in order to study the property of the signal recreated at the source location (time compression) and the spatial property of the time-reversed wave around the source location (spatial focusing), leading to the first demonstration of the reversibility of an acoustic wave propagating through a random collection of scatterers with strong multiplescattering contributions. It has been observed that, after time reversal, the waves travel on the same scattering paths and focus back on the source as if they were passing through a converging lens. Because of the scattering sample, higher spatial frequencies than in a purely homogeneous medium can be detected. High spatial frequencies that would have been lost otherwise are redirected due to the presence of the scatterers in a large area. These experiments show also that the acoustic time-reversal

experiments are surprisingly stable.

3.2.4 Time Reversal as time correlator

Like any linear and time-invariant process, wave propagation through a multiple-scattering medium may be described as a linear system with different impulse responses [7]. If a source, located at $\vec{\mathbf{r}}_0$, sends a Dirac pulse $\delta(t)$), the j-th transducer of the TRM will record the impulse response $h_j(t)$ that corresponds, for a point transducer located at $\vec{\mathbf{r}}_j$, to the Green function $\mathbf{G}(\vec{\mathbf{r}}_j, t|\vec{\mathbf{r}}_0, 0)$. Moreover, due to reciprocity, $h_j(t)$ is also the impulse response describing the propagation of a pulse from the j-th transducer to the source. Thus, neglecting the causal time delay T, the time-reversed signal at the source is equal to the convolution product $h_j(t) * h_j(-t)$. This convolution product, in terms of signal analysis, is typical of a *matched filter*. Given a signal as input, a matched filter is a linear filter whose output is optimal in some sense. Whatever the impulse response $h_j(t)$, the convolution $h_j(t) * h_j(-t)$ is maximum at time $t = 0$. This maximum is always positive and is equal to $\int h_j^2(t)dt$, i.e. the energy of the signal $h_j(t)$. This has an important consequence. Indeed, with an N-element array, the time-reversed signal recreated on the source is written as a sum:

$$\Phi^{tr}(\vec{r}_0, t) = \sum_{j=1}^{N} h_j(t) * h_j(-t)$$

Even if the $h_j(t)$ are completely random and apparently uncorrelated signals, each term in this sum reaches its maximum at time t=0, so all contributions add constructively around t=0, whereas at earlier or later times uncorrelated contributions tend to destroy one another. Thus the re-creation of a sharp peak after time reversal on an N-element array can be viewed as an interference process between the N outputs of N matched filters, as shown in Fig. 3.7:

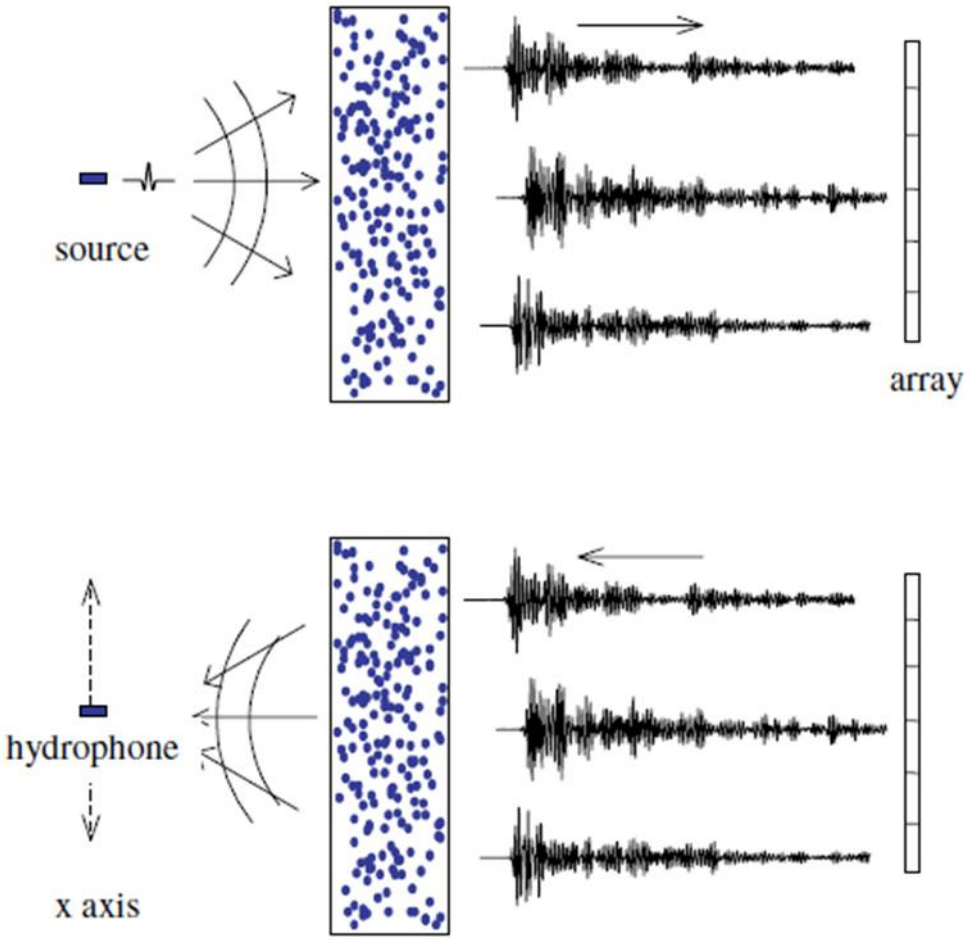

Fig. 3.6: Sketch of time-reversal experiment through a random medium. Figure taken from [7].

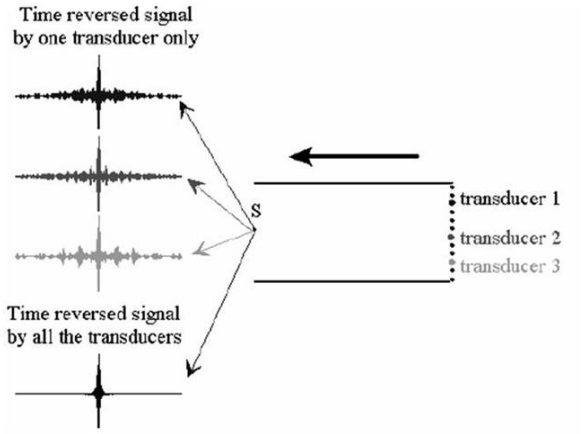

Fig. 3.7: Contribution of each transducer of TRM to Time Reversed field [7].

each individual contribution of the time-reversed field is a symmetrical signal with a maximum at the same time T for each transducer. When all the transducers of the TRM work together the summation of all the signals give a perfect time recompression at the origin [7].

The robustness of the TRM can also be accounted for through the matched filter approach. If we take into account additional noise on channel j, $n_j(t)$, then the re-created signal is written:

$$\sum_{j=1}^{N} h_j(t) * h_j(-t) + \sum_{j=1}^{N} h_j(t) * n_j(t)$$

The time-reversed signals $h_j(-t)$ are tailored to exactly match the medium impulse response, which results in a sharp peak, whereas an additional small noise is not matched to the medium and, given the extremely long duration involved, it generates a low-level long-lasting background noise instead of a sharp peak.

3.2.5 Time Reversal as spatial correlator

Another way to consider the focusing properties of the time-reversed wave is to follow the impulse response approach and treat the time-reversal process as a spatial correlator [7]. If we denote by $h_j(t)$ the propagation impulse response from the $j-th$ element of the array to an observation point $\vec{r}_1$ different from the source location $\vec{r}_0$, the signal recreated in $\vec{r}_1$ at time $t_1 = 0$ is written:

$$\Phi_j^{tr}(\vec{r}_1, 0) = \int h_j(t) * h_j^{'}(t)dt$$

Notice that this expression can be used as a way to define the directivity pattern of the time-reversed waves around the source. Now, due to reciprocity, the source S and the receiver can be exchanged, i.e. is also the signal that would be received in $\vec{r}_1$ if the source were the $j-th$ element of the array. Finally, the fundamental properties of time reversal rely on the fact that it is both a space and time correlator, and the time-reversed waves can be viewed as an estimate of the space and time auto correlation functions of the waves scattered by a random medium. The estimate becomes better with a large number of transducers in the mirror. Moreover, the system is not sensitive to a small perturbation since adding a small noise to the scattered signals (e.g. by digitizing them on a reduced number of bits) may alter the noise level but does not drastically change the correlation time or the correlation length of the scattered waves. Even in the extreme case where the scattered signals are digitized on a single bit, Derode et al. have shown that the time and space resolution of the TRM are practically unchanged, which is striking evidence for the robustness of wave time reversal in a random medium [3].

3.2.6 Time reversal in chaotic cavities

Another important experiment regarding the use of TR in acoustics has been carried out considering waves confined in closed reflecting cavities such as elastic waves propagating in a silicon wafer. With such boundary conditions, no information can escape from the system and a reverberant acoustic field is created. If, moreover, the cavity shows ergodic properties (an acoustic ray would pass every location in the cavity after multiply reflections) and negligible absorption, one may hope to collect all information at only one point. Draeger and Fink have shown experimentally and theoretically that in this particular case a time reversal can be obtained using only one TR channel operating in a closed cavity. The field is measured at one point over a long period of time and the time-reversed signal is re emitted at the same position. The experiment is two dimensional and has been carried out by using elastic surface waves propagating along a monocrystalline silicon wafer whose shape is a chaotic stadium. The shape of the cavity is of crucial importance. The chaotic stadium geometry ensures that each acoustic ray radiated by the source will pass, after several reflections, sufficiently close to any point of the cavity. This ergodic property may be obtained for different geometries, and the selected geometry, called a "D-shape stadium", was chosen for its simplicity. Silicon was selected for its weak absorption. An aluminium cone coupled to a longitudinal transducer generates these waves at one point of the cavity. A second transducer is used as a receiver. In the first step of the experiment, one of the transducers, located at point A, transmits a short omnidirectional signal of duration 0.5 μs into the wafer. Another transducer, located at B, observes a very long chaotic signal, that results from multiple reflections of the incident pulse along the edges of the cavity, and which continues for more than 50 ms, corresponding to some hundred reflections

along the boundaries. Then, a portion of 2 ms of the signal is selected, time reversed and re-emitted by point B. One observes both an impressive time recompression at point A and a refocusing of the time-reversed wave around the origin (Fig. 3.8 (a) and (b)) with a focal spot whose radial dimension is equal to half the wavelength of the wave. Using reflections at the boundaries, the time-reversed wavefield converges towards the origin from all directions and gives a circular spot, like the one that could be obtained with a closed cavity covered with transducers (see Fig. 3.2.1). The success of this time-reversal experiment is particularly interesting with respect to two aspects. Firstly, it proves again the feasibility of time reversal in wave systems with chaotic ray dynamics. Paradoxically, in the case of one channel time reversal, chaotic dynamics is not only harmless but also even useful, as it guarantees ergodicity. Secondly, using a source of vanishing aperture, we obtain an almost perfect focusing quality. The procedure approaches the performance of a closed Time Reversal Cavity, which has an aperture of 360. Hence, a one-point time reversal in a chaotic cavity produces better results than a TRM in an open system. Using reflections at the edge, focusing quality is not aperture limited and, in addition, the time-reversed collapsing wavefront approaches the focal spot from all directions.

3.2.7 Iterative Time Reversal in pulse-echo mode

One of the most promising areas for the application of TRMs is pulse-echo detection [7]. In this domain, one is interested in detection, imaging and even destruction of passive reflecting targets. In general, the acoustic detection efficiency depends on the ability to focus a beam in the medium of interest. The presence of sound speed fluctuations between the targets and the transducers can drastically change the beam profiles. In medical applications,

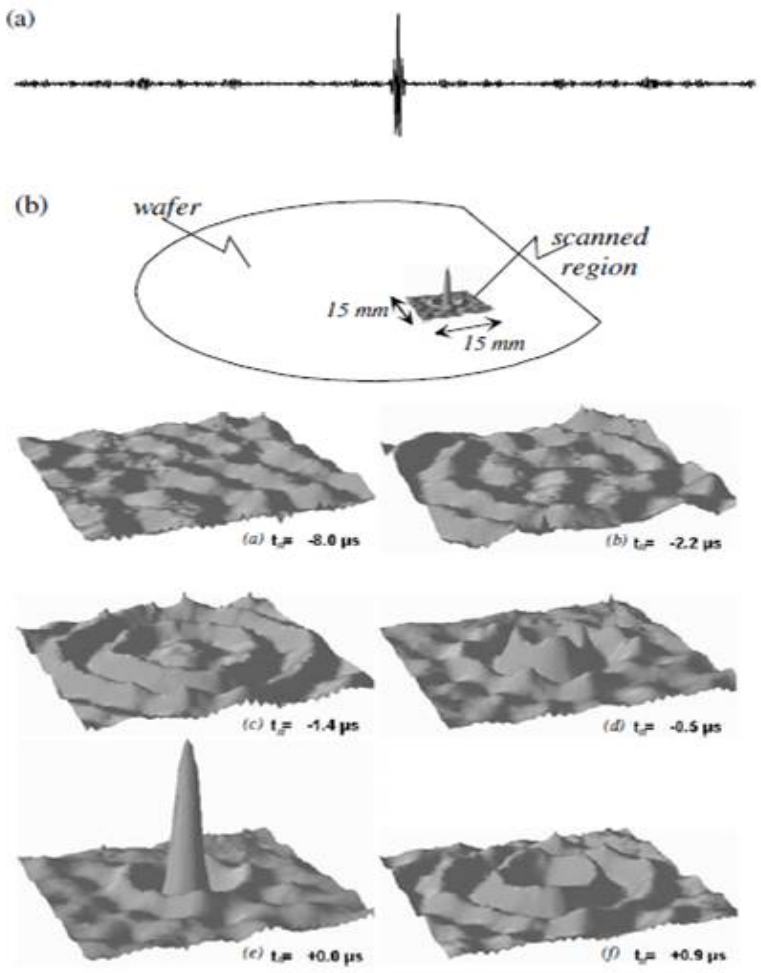

Fig. 3.8: (a) Time-reversed signal observed at point A. The observed signal is 210 μs long. (b) Time-reversed wavefield observed at different times around point A [7].

one looks for organ walls, calcification or kidney stones, and a fat layer of varying thickness, bone tissues or some muscular tissues may greatly degrade focusing. In underwater acoustics, the objects to detect can be submarines, or mines eventually buried under sediments. In this case, refraction due to oceanic structure ranging in scale from centimetres to tens of kilometres is an important source of distortions. For all these applications, a TRM array can be controlled according to a three-step sequence. One part of the array generates a brief pulse to illuminate the region of interest through the distorting medium. If the region contains a point reflector, the reflected wavefront is selected by means of a temporal window and then the acquired information is time reversed and re-emitted. The re-emitted wavefront refocuses on the target through the medium. It compensates also for unknown deformation of the mirror array. As has been shown the TR processing is a realization of the spatiotemporally matched filter to the propagation transfer between the array and the target. Although the time-reversal self-focusing technique is highly effective, it requires the presence of a reflecting target in the medium. When this medium contains several targets, the problem is more complicated and iteration of the TR operation may be used to select one target. Indeed, if the medium contains two targets of different reflectivity, the time reversal of the echoes reflected from these targets generates two wavefronts focused on each target. The mirror produces the real acoustic images of the two reflectors on themselves. The highest-amplitude wavefront illuminates the most reflective target, while the weakest wavefront illuminates the second target. In this case, the time-reversal process can be iterated. After the first time-reversed illumination, the weakest target is illuminated more weakly and reflects a fainter wavefront than that from the strongest target. After some iterations, the process converges and produces a wavefront focused on

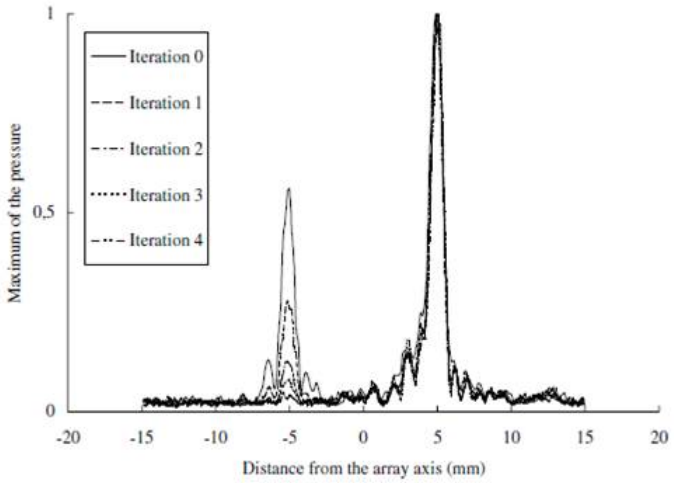

Fig. 3.9: Iterative TR experiment: pressure measured in the wire plane after each iteration [7].

the most reflective target if the target separation is sufficient to avoid the illumination of one target by the real acoustic image of the other one. Experiments have been performed with a linear array of 128 transducers. The scatterers were 0.2 mm and 0.4 mm diameter copper wires separated by 10 mm and placed at 90 mm distance perpendicular to the array. A rubber aberrating layer was placed between the array and the two wires. In the first step, the beam was transmitted by a single transducer element located at the array centre. After the first illumination, the echoes from the two targets were recorded. The recorded signals were then time reversed and retransmitted and this process iterated four times. Fig. 3.9 represents the pressure field, which shows two maxima corresponding to the two target locations. The pressure field reaches a higher value at the location of the wire of larger scattering cross section. As the process was iterated the weaker wire received a weaker time reversed wave. The smallest wire is no longer illuminated after the fourth illumination. In general, the iterative TR process is not trivial

and many studies have been conducted by Fink et al. on the convergence of TR iterations in a multiple-target medium and the conditions for selecting the most reflective targets have been derived [7].

3.3 Time Reversal in UWB

Because of its simplicity and performance advantages, the idea of applying the TR in wireless communication has gained much attention recently. In fact, the use of TR has many benefits in communications. Temporal focusing significantly shortens the effective length of the channel. For example, the complexity of a MLSE equalizer is exponential in the length of the channel. TR reduces therefore the complexity of the equalization task. A more important advantage of the TR technique is spatial focusing, that results in very low cochannel interference in a multi-cell system [1]. This results in a very efficient use of bandwidth in the overall system. The application of TR in impulse radio UWB transmission is a possible solution to improve the multiuser system capacity. It is expected that the extremely wide bandwidth of the UWB signal will help in increasing the temporal compression and in improving the spatial focusing characteristics of TR. On the other hand, TR may help in reducing the complexity of the receiver devices and in lowering the required transmitting power in an UWB system. This aspect will be investigated in **Chapter 4**.

Emami et al. demonstrated the remarkable space-time focusing properties of UWB signal transmission with time reversal using broadband radio wireless measurements in an indoor environment. They showed the remarkable space-time focusing properties of signal transmission with time reversal. In the TR scheme proposed by the auhors, they considered a transmitter/re-

ceiver pair and they measured the channel impulse response between the transmitter and a receiver, repeating the measurement changing the position of the receiver (the transmitter has been kept fixed). If $h(\vec{r}_0, \tau)$ is the channel impulse response, where $\vec{r}_0$ is the receiver location and τ the variable delay, the time reversed complex conjugate of the channel impulse response $h^*(\vec{r}_0, \tau)$ is used as a transmission prefilter [6]. In order to show the spatial focusing property of the TR-UWB scheme, the power of the signal as a function of both space and delay has been computed and investigated by the authors, using the following quantity as spatial focusing metric:

$$k(\mathbf{r}) = max_\tau \left| s(\mathbf{r}, \tau) \right|^2$$

This quantity represents the power of the strongest tap at a receiver located at $\mathbf{r}$. The measurement has been conducted in the following way: the environment is an office space (40m x 60m) with many cubicles. Measurements span the bandwidth 2-8 GHz with 3.75 MHz frequency resolution. From the data they estimate that the coherence bandwidth of the channel is 20 MHz. Antennas are vertically polarized. The virtual grid on which the receiver is moved has a distance of $\lambda_0/4$, where λ_0 is the wave length of the mid frequency of the measurements (5 GHz). The receiver antenna is moved to a different location with a precise robotic positioner. At each antenna position, the channel is measured using a vector network analyser. The measurements are corrected to compensate for the system components (including cable, gain stages, and antennas). The height of the transmit antenna is about 2.5 m and that of the receive antenna is 1m above the floor. The 3D plot of $k(\mathbf{r})$ in Fig. 3.10, shows that spatial focusing works fine in both LOS and NLOS scenarios. In the 3-D figures, the square grid spans a region of $7\lambda_0 \times 7\lambda_0$. However, the peaks are not isotropic, but they have one direction in which they fall off faster, and another, in which the decay is slower. The structure

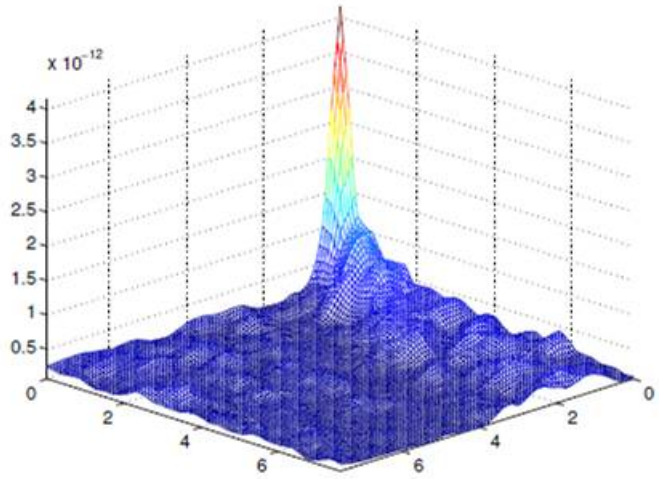

(a) Case I

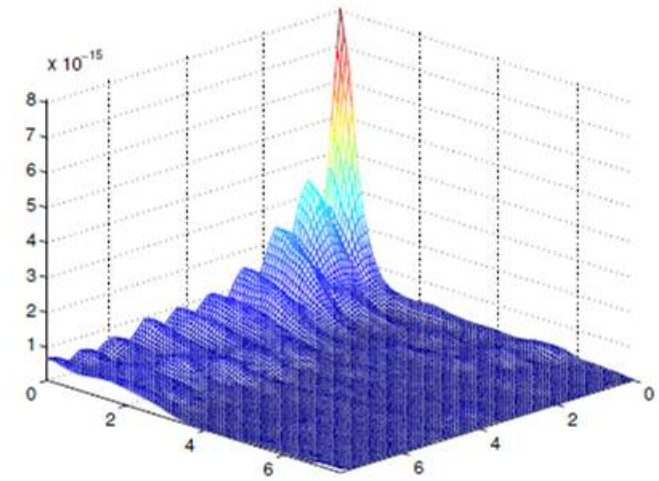

(b) Case II

Fig. 3.10: Spatial focusing of TR. One shot spatial field realizations for (a) the line-of-sight (b) the non-line-of-sight scenario. Figure taken from [6].

of the peak carries some information about the geometry of the environment, i.e., about directions which show faster and those which show slower decorrelation in space. We also observe that the signal power level is at least 10dB lower at a distance of $7\lambda_0$ than its value at the receiver. This demonstrates the spatial decorrelation very well. We can conclude that channel impulse responses show inherent quasi-orthogonality in space, which can be used for interference suppression. This experiment shows that the benefits of TR, which have been observed in acoustic TR experiments, could also be gained in wireless communications. These results have been confirmed by another experiment carried out by Akogun et al., that, employing a time-domain channel sounding technique to obtain the UWB channel information in typical LOS and NLOS cases, demonstrated temporal compression and spatial focusing performed by using TR in UWB [1]. To characterize the amount of temporal focusing, they defined a ratio called the temporal peak to total energy ratio, which characterizes the percentage energy capture, by the peak of the effective Channel Impulse Response (CIR):

$$\vartheta^{TR} = \frac{E_P^{hh}}{E_T^{hh}}$$

where E_P^{hh} is the energy of the main peak of the received impulse response and E_T^{hh} is the total energy in the received impulse response for the timereversed channel. To illustrate temporal compression in TR, the authors computed the temporal peak to total energy ratio ϑ^{TR} for LOS and NLOS at distances of 10 m away from the transmitter, seeing that ϑ^{TR} is higher for the NLOS case compared to the LOS case. For the LOS case reported in [1], ϑ^{TR} is about 59.96% while the NLOS case has a ϑ^{TR} value of about 65.73%. This shows that temporal compression works finer for the NLOS scenarios compared to the LOS scenario. These results show again that TR is an effective way to reduce the delay spread in a UWB channel and also demonstrated security

in TR. In fact, at about 6m away from the intended receiver, the spatial focusing gain observed is at least 10 dB: this means a very low probability of intercept by a nearby receiver [1].

3.3.1 Performance of TR-UWB-IR

As said, the temporal focusing and the spatial focusing of time reversal make the energy collection increase and improve the performance of an UWB system. In this section we present the results obtained by Liu et al. [15], that evaluated the bit-error-rates performance of impulse radio ultra-wideband (IR-UWB) wireless communication system based on time reversal technique, in four typical line of sight (LOS) and non line of sight (NLOS) IEEE 802.15.3a scenarios. The communication system has been simulated and the bit-error-rates (BER) versus the signal-to-noise ratio (Ex/No) have been investigated. The results obtained have been compared with the results given by UWB system with S-RAKE receiver. A repetition code for the input data stream is generated by the repetition coder to efficiently improve the BER performances of both traditional UWB system and TR UWB system. TH-PPM scheme and DS-PAM scheme are employed and evaluated. The basic simulation parameters are: sampling frequency $f_s = 50$ GHz, average transmitted power $A_{pow} = -30$ dB, average pulse repetition period $T_s = 60$ ns, number of pulses per bit $N_s = 9$, PPM time shift $d_{PPM} = 0.5$ ns, chip time for TH-PPM $T_c = 1$ ns, periodicity of TH code for TH-PPM $Npth = 5$, cardinality of the TH code $N_c = 5$, periodicity of DS code $Npds = 10$. It has been observed that the TR based SISO system, as expected, has much better BER performance than usual UWB system in all four channels and in both TH-PPM and DS-PAM cases. Performances with 6, 9 and 15 users have been investigated. The BER performances using the TH-PPM scheme are shown

in Fig. 3.11. The results hold the promise of the TR based UWB systems.

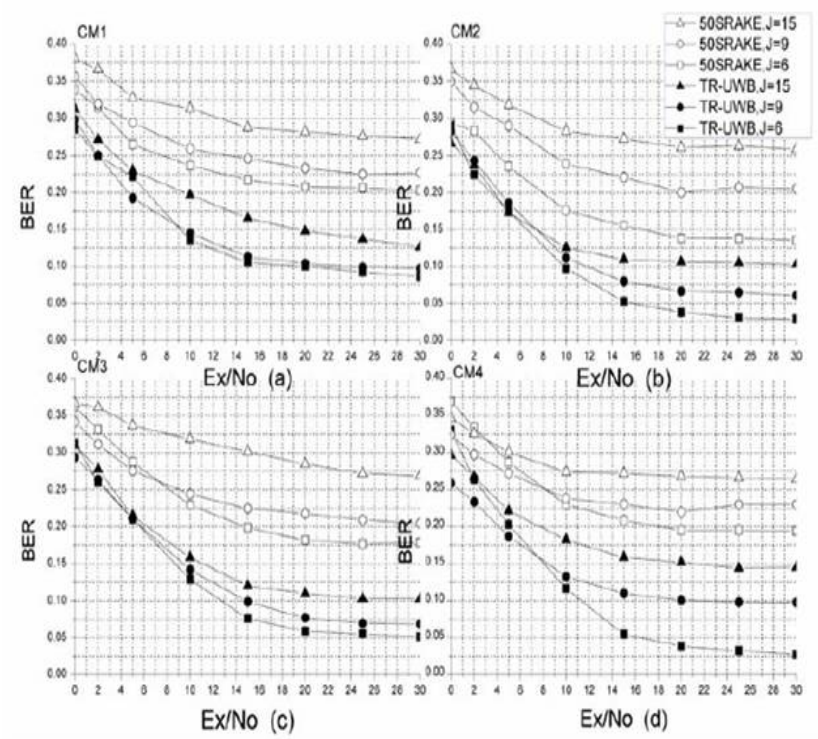

Fig. 3.11: BER performances (using TH-PPM scheme) of multi-user TR-IR-UWB system and usual UWB system. Figure taken from [15].

From the observation of Fig. 3.11 we could answer how many Rake fingers should be used if usual systems want to get as good performance as a TR based system. The trade-off between the number of fingers in the prefilter of a TR-IR-UWB system versus the number of fingers in the rake receiver has been investigated by Panaitopol et al. As we said, Time Reversal (TR) IR-UWB systems use a prefilter at the transmitter side, that has the function of convolving the UWB pulse with the impulse response of the channel reverted in time; when the signal traverses the channel, the output of the channel presents the correlation of the channel with itself. Thus, the Time Reversal prefilter has a function somehow analog to the rake receiver i.e.

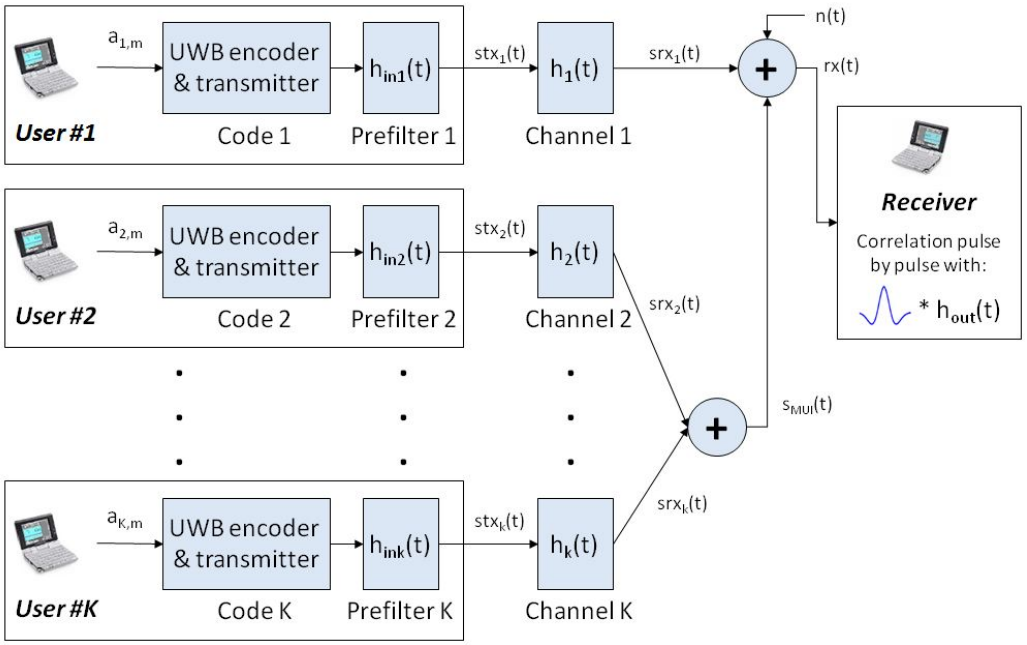

Fig. 3.12: General tx/rx scheme for a TR-IR-UWB system

creating the correlation of the channel with itself. As a matter of fact one of the main advantages which is often claimed for TR is to move the complexity from the receiver to the transmitter. Moreover, like the rake receiver, the rake of the prefilter at the transmitter side may be implemented 'partially' by selecting a number of fingers lower than the total number of paths in the channel, reducing thus the complexity of implementation. As a matter of fact, while using TR, the receiver should still use a rake adapted to the new signal, so the general tx/rx chain of Fig. 2.2 changes in the way shown in Fig. 3.12, where $h_1(t)$, $h_2(t)$, ..., $h_k(t)$ are the channel impulse responses of the different users. The general expression for one of these multipath channels is as follows:

$$h_k(t) = \sum_{i=0}^{L} \gamma_{k,i} \delta(t - \tau_{k,i})$$

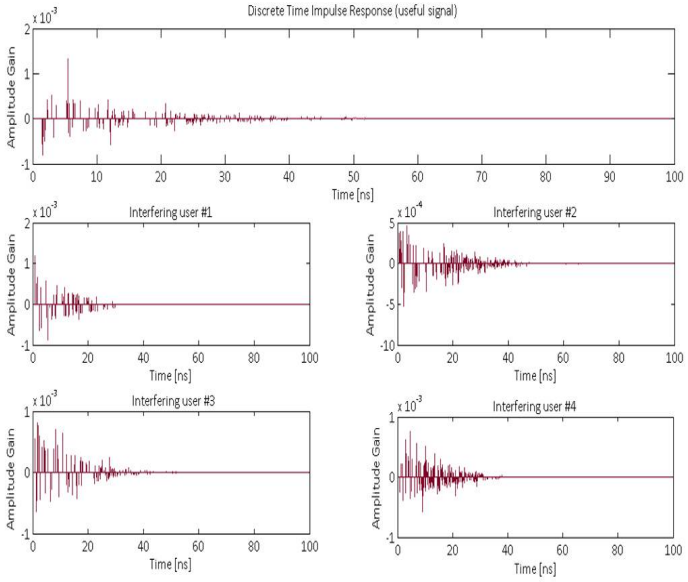

Fig. 3.13: Examples of IEEE 802.15.3a channels for 5 users.

with L the total number of paths in the channel, τ_i the delay of the $i-th$ path and γ_i its amplitude (see Fig. 3.13); $h_{in,1}(t)$, $h_{in,2}(t)$, ..., $h_{in,k}(t)$ are the transmission prefilters. To reduce the complexity only a subset of paths could be considered [17], then the general expression of the impulse response of the k-th prefilter is:

$$h_{in,k}(t) = \sum_{i=0}^{N_{in-1}} \alpha_{k,i}\delta(-(t-\tau_{k,i}))$$

with $N_{in} \leq L$ the number of the strongest paths to consider. An example of $h_{in}(t)$ is shown in Fig. 3.14. $h_{out}(t)$ is a selection of $N_{out} \leq 2L$ paths of the equivalent TR channel, namely $h_{in}(t) * h(t)$. It is obtained by the selection of the N_{out} strongest paths of equivalent TR channel, as shown in Fig. 3.15 Making the correlation between the received signal and $\omega(t) * h_{out}(t)$, where $\omega(t)$ is the unit-energy basic pulse waveform of duration $T_M < T_c$, means to implement a Selective Rake receiver (the All Rake has to perform the

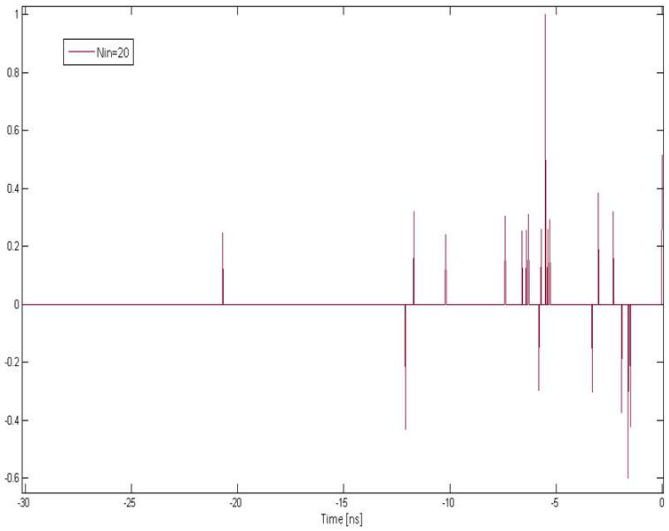

Fig. 3.14: Impulse response of transmission prefilter with $N_{in} = 20$ fingers.

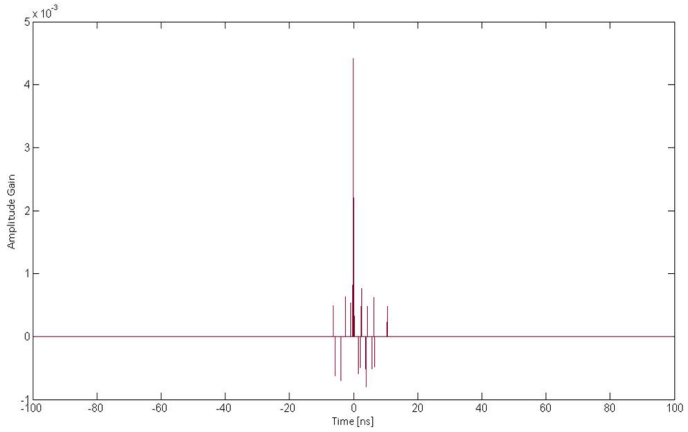

Fig. 3.15: Example of $h_{out}(t)$ with $N_{out} = 20$ fingers

correlation of the received signal with $\omega(t) * h_{in}(t) * h_(t))$. As a matter of fact, while using TR, the receiver should still use a rake adapted to the new signal. In [17], the authors analyzed the BER as a function of the number of fingers in the prefilter N_{in} and in the rake receiver N_{out}. The N selected paths from the fingers correspond to the N strongest ones (S-RAKE).

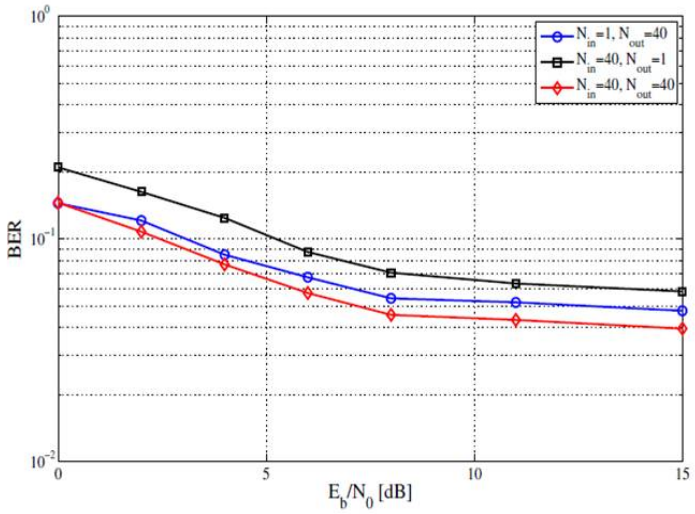

Fig. 3.16: TR-UWB-IR performance with strong interference from 5 users with 10 dB above the useful signal. Figure taken from [17].

Performance changes when switching the number of fingers from the receiver to the transmitter. For instance, when $N_{in} = 1$ and $N_{out} = 10$ (i.e. without time reversal) performance is better than when $N_{in} = 10$ and $N_{out} = 1$. In order to keep same performance when the number of fingers at the rake receiver is lowered, the number of fingers at the transmitter must be increased in a more important way, and a small number of fingers has still to be kept at the receiver. This can be explained by a major spreading of the energy on various paths: while the main path is strongest in time reversal, many sub paths may appear, creating thus a major energy spreading [17].

As expected, increasing the number of fingers in the rake receiver while keeping a fixed number of fingers at the prefilter always increases performance. The results show that time reversal helps moving complexity from receiver to transmitter, only when receiver has initially a low number of fingers, otherwise the use of time reversal with reduced fingers at the rake receiver reduces performance. The impact of time reversal is more promising however, in a scenario with Multi-User Interference. Fig. 3.16 shows that time reversal may lead to better performance in the case of sttrong interferers: see $N_{in} = 1$, $N_{out} = 40$ versus $N_{in} = 40$, $N_{out} = 40$. This happens due to the fact that TR modifies the MUI distribution, while, as we have seen, the MUI distribution may have a strong impact on the IR UWB performance.

This aspect is the main topic of this work and will be deeply investigated in **Chapter 4**.

Chapter 4

Impact of Time Reversal on Multi-User Interference

In this chapter we show how the Time Reversal technique, applied to UWB-IR systems, has an impact on the distribution of multi-user interference and how performance may benefit from this MUI distribution change, that has been studied in several reference scenarios with multipath channels, varying the transmission parameters (number of users, power trasmitted by intended and interfering transmitters, repetition code) in various network topologies. We underline the limits of validity of Standard Gaussian Approximation for the MUI distribution and that the use of Time Reversal, in a UWB-IR communication system affected by multi-user interference, leads to improved performance both with a classical rake receiver and with a receiver adapted to a Generalized Gaussian distribution. The study has been performed in several cases in which the TR technique has been used in a more or less deep way. As said, in order to apply the Time Reversal technique to UWB systems, we need to use transmission pre-filters to convolve the UWB pulse with the channel impulse response, inverted in time. In a multi-user

system that makes use of TR, the time-reversed channel impulse response of any link between receiver and active users is taken as a prefilter at the transmitter [21]. In this way, when the transmitted signals pass through the equivalent channel, represented by the convolution $h(-t) * h(t)$, the output of the channel presents the correlation of the channel with itself. Thus, the Time Reversal prefilter has a function somehow analog to the rake receiver i.e. creating the correlation of the channel with itself. Our study aims to investigate how the use of this technique in UWB-IR systems changes the MUI distribution, that often is modeled by a Standard Gaussian for reasons of simplicity (Standard Gaussian Approximation, SGA). However, this approximation is often not valid even with a classic system [4] [5] [11], and it turns out even less accurate if we use TR. In fact, due to the impulsive nature of UWB signals, SGA approximation is often not enough accurate even for classic UWB-IR schemes, and due to temporal focusing introduced by TR this aspect becomes even more marked. In the first part of our study we verify by simulations that the MUI distribution is more and more far from a Standard Gaussian when the impact of TR on the system increases. We consider the kurtosis as the reference parameter of the distribution of the variable associated to MUI at the correlator output, and we show that this parameter tends to increase if a more deep TR configuration is used, resulting in a more tight distribution than a classical Gaussian one with same variance. This interesting aspect has been used in the second part of our study, in which we replace the classical correlation receiver with one adapted to a Generalized Gaussian distribution, according to [10], verifying a performance enhancement with the adapted receiver. We also carried out a comparison between the performance achieved using a classical rake receiver without TR, those in presence of a classical rake receiver when TR is used and those

achieved using the adapted receiver in combination with TR, showing (and explaining the reasons of) an improvement of performance in terms of BER vs. SNR obtained when we use TR both with classical and with adapted receivers, even in presence of strong interferers.

4.1 Signal model

We consider in this work a Pulse Position Modulation Time Hopping Ultra Wide Band system (PPM-TH-UWB) [4]. The general tx/rx scheme for a multi-user UWB system that makes use of Time Reversal considered in our simulations and modeled in MATLAB is that of Fig. 3.12. We use a repetition code, so N_s pulses for the same information bit are transmitted in order to increase the robustness of the system (but other channel codes could be used). Without Time Reversal, the signal sent by user k may be written as:

$$s_{tx_k}(t) = \sqrt{\frac{E_{tx_k}}{N_s}} \sum_m \sum_{j=0}^{Ns-1} w(t - mN_sT_s - jT_s - c_{(k,mN_s+j)}T_c - d_{PPM}a_{k,m})$$

Where $w(t)$ is the unit-energy basic pulse waveform, K is the number of users simultaneously active, $a_{k,m}$ the information symbol transmitted by user k during the symbol interval m, repeated over N_s frames of duration $T_s = N_hT_c$ each, where T_c is the so-called chip interval and N_h is the number of slots per frame [4]. The time hopping code assigned to each user is a pseudo-random sequence $(c_{k,l}^{(K)})_{l\in\mathbb{Z}}$ and from the point of view of other users it may be modelized as a collection of independent random variables, distributed in $0, \ldots, N_h - 1$. E_{tx_k} is the energy sent for each bit. We consider one receiver and we note $h_1(t)$, $h_2(t)$, $\ldots$, $h_k(t)$ the channel impulse responses of the

different transmitting users. The principle of Time Reversal is to convolve the pulse by an inverted version of the channel before to send it, so the propagation of the signal through the channel will have the effect to receive the channel correlated to itself (thus simulating a correlation receiver). So with perfect Time Reversal the signal sent by user k can be written as:

$$s_{trtx_k}(t) = \sqrt{\frac{E_{trtx_k}}{N_s}} \sum_{m} \sum_{j=0}^{Ns-1} h_k(-t) * w(t - mN_sT_s - jT_s - c_{(k,mN_s+j)}T_c - d_{PPM}a_{k,m})$$

E_{trtx_k} sets the energy sent by bit (it is not directly the energy per bit as the convolution by $h_k(t)$ has to be taken into account). The general expression for one of the multipath channels is as follows:

$$h_k(t) = \sum_{i=0}^{L} \gamma_{k,i}\delta(t - \tau_{k,i})$$

with L the total number of paths in the channel, τ_i the delay of the $i-th$ path and γ_i its amplitude; $h_{in,1}(t)$, $h_{in,2}(t)$, ..., $h_{in,k}(t)$ are the transmission prefilters with $h_{in,k}(t) = h_k(-t)$. However, to reduce the complexity of the transmitter we could reduce the number of path considered in $h_{in,k}(t)$, selecting only the N_{in} strongest path.

An all rake receiver synchronized on user 1 has now to perform the correlation of the received signal $rx(t)$ with $\omega(t) * h_{in,1}(t) * h_1(t)$. Without loss of generality, we consider the symbol m=0 for user 1, so we drop this index for this user. The output of the pulse-by-pulse correlator can be written as:

$$r_{imp}[n] = \int rx(t) \cdot (h_{out}(t)*(w(t - nT_s - c_{1,n}T_c) - w(t - nT_s - c_{1,n}T_c - d_{PPM})))dt$$

The classical receiver will make its decision on the received symbol based on the sign of $\sum_{n=0}^{n=N_s-1} r_{imp}[n]$. For the all rake $h_{out} = h_{in,1}(t) * h_1(t)$. But

in order to reduce the receiver complexity, a partial rake may be used were h_{out} will consider only a sub set of N_{out} path of $h_{in,1}(t) * h_1(t)$. Making the correlation between the received signal and $w(t) * h_{out}(t)$ means to implement a Selective Rake receiver (the All Rake has to perform the correlation of the received signal with $w(t) * h_{in}(t) * h(t)$). As a matter of fact, while using TR, the receiver should still use a rake adapted to the new signal. Assuming the perfect synchronization between the receiver and the user k, its contribution to the received signal can be written as follows:

$$s_{rx_k}(t) = \sqrt{\frac{E_{rx_k}}{N_s}} \sum_{m} \sum_{j=0}^{Ns-1} g_k(t - mN_sT_s - jT_s - c_{(k,mN_s+j)}T_c - d_{PPM}a_{k,m})$$

In this expression, $g_k(t) = h_{TR}(t) * \omega(t)$, where $h_{TR}(t) = h_{in} * h(t)$, the equivalent Time Reversal channel, composed by the cascade of transmission pre-filter and multipath channel associated to user k, while E_{rx_k} represents the mean energy per received bit for user k and d_{PPM} is the shift introduced by the Pulse Position Modulation. We denote by $s_{MUI}(t)$ the contribution of multi-user interference to received signal: $s_{MUI}(t) = \sum_{k=2}^{K} s_{rx_k}(t - \Delta_k)$, where Δ_k represents the relative delay, less than a frame duration Ts, of user k with respect to the reference signal of user 1, due to the absence of synchronization between the various users. If we assume perfect synchronization between receiver and reference transmitter, the received signal can be expressed in the following way:

$$rx(t) = s_{rx_1}(t) + s_{MUI}(t) + n(t)$$

Where $n(t)$ is Additive White Gaussian Noise (AWGN). The pulse-by-pulse correlator output is as follows:

$$r_{imp}[n] = r_{imp,u}[n] + r_{imp,MUI}[n] + r_{imp,AWGN}[n]$$

The receiver operates a soft decision on the bit received, as shown in Fig. 4.1.

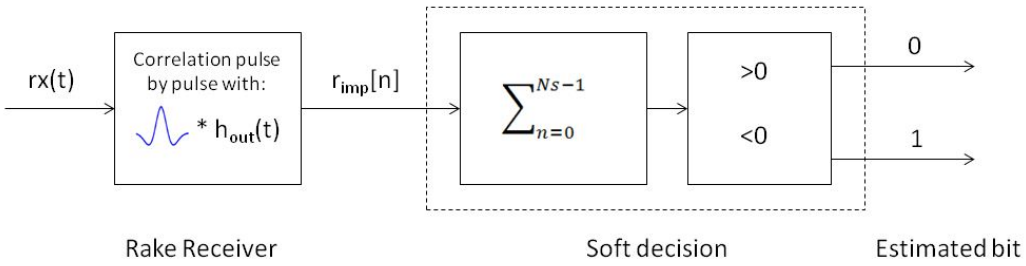

Fig. 4.1: Classical 2-PPM-UWB rake receiver.

4.2 Impact of TR on MUI distribution

It has been proved that MUI distribution is not Gaussian in several cases and that the Gaussian approximation is often not valid in UWB-IR systems [4] [5] [11], this is due to the impulsive nature of UWB signals. The SGA is even less accurate is we consider a UWB-IR transmisssion scheme that makes use of Time Reversal. In this case, the MUI distribution is more and more far from a Standard Gaussian if the impact of TR increases, that is, the number of fingers of transmission pre-filters grows. We consider the kurtosis $k = \frac{E[x^4]}{E[x^2]^2}$ of the MUI distribution as the reference parameter to show the MUI distribution similarity with a Gaussian. Kurtosis is a measure of how outlier-prone a distribution is. Kurtosis of the normal distribution is 3: distributions that are more outlier-prone than the normal distribution have kurtosis greater than 3; distributions that are less outlier-prone have kurtosis less than 3. The kurtosis of the MUI distribution increases more and more with the impact of TR on the system, resulting in a more tight distribution

than a classical Gaussian one with same variance. If we reduce the number of fingers in TR pre-filters, the MUI distribution approaches increasingly a Gaussian. This aspect has been confirmed by simulations: as expected, since the fingers of the transmission pre-filter decrease, the impact of TR is less significant and the kurtosis of the distribution is closer to 3. So the SGA in a system that makes use of TR techinque is less accurate with respect to the traditional non-TR scheme, leading to a too optimistic estimate of classical correlation receiver performance. We could model MUI with a more appropriate distribution, using the Generalized Gaussian to better fit the MUI distribution [10]. The expression of this distribution is as follows:

$$p(x) = \frac{c_1(\beta)}{\sqrt{\sigma^2}} exp(-c_2(\beta) \left| \frac{x}{\sqrt{\sigma^2}} \right|^{\frac{2}{1+\beta}})$$

with

$$c_1(\beta) = \frac{\Gamma^{\frac{1}{2}}(\frac{3}{2}(1+\beta))}{(1+\beta)\Gamma^{\frac{3}{2}}(\frac{1}{2}(1+\beta))}$$

and

$$c_2(\beta) = (\frac{\Gamma(\frac{3}{2}(1+\beta))}{\Gamma(\frac{1}{2}(1+\beta))})^{\frac{1}{1+\beta}}$$

The relation between the kurtosis k and the coefficient β is as follows:

$$k = \frac{\Gamma(\frac{5(1+\beta)}{2})\Gamma(\frac{(1+\beta)}{2})}{(\Gamma(\frac{3(1+\beta)}{2}))^2}$$

A receiver adapted to a Generalized Gaussian interference has been proposed by [12]. This receiver consists in the insertion of a non-linear limiter that takes into account the parameter β. Then, the expression of the limiter function h_l is:

$$h_l(r) = 0.5^{\frac{2}{1+\beta}}(|r+1|^{\frac{2}{1+\beta}} - |r-1|^{\frac{2}{1+\beta}})$$

In Fig. 4.2 we can see the scheme of the adapted receiver.

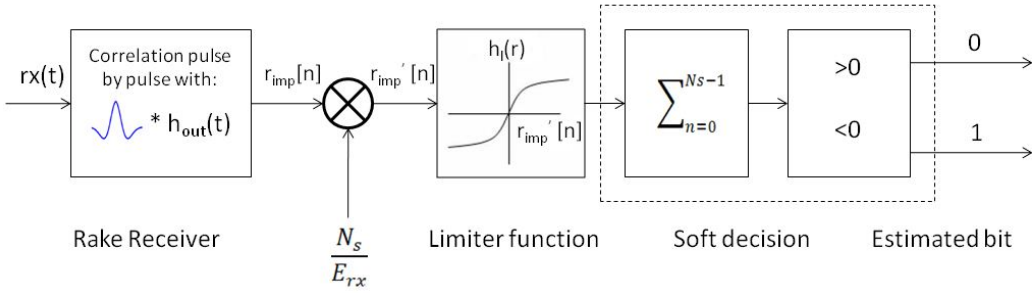

Fig. 4.2: 2-PPM-UWB correlation receiver adapted to a Generalized Gaussian MUI.

4.3 Simulation results

At first, the K users are distributed in the network according to a star topology, where the distance from the receiver is 10 meters for both the intended transmitter and interfering users. The kurtosis of the multi-user interference signal distribution resulting from simulations was calculated after having transmitted 20000 bits, over a number of loops that varies in relation to the robustness of the repetition coder (a stronger repetition code corresponds to a longer signal). At each loop, the system generates and transmits K signals according to the 2-PPM-TH-UWB transmission technique. We have supposed a perfect synchronization between receiver and intended transmitter. It is remarkable the fact that the use of TR transmission prefilters causes a temporal shift in received signal (see Fig. 4.3), resulting in a misalignment between the received signal and the correlator mask. This shift has been compensated in simulations at receiver side. The different users are asynchronous: they don't know when the frame associated to the reference user begins. In order to consider this asynchronism, that leads to a loss of orthogonality between the TH codes, a random delay is introduced at each loop, so each interfering signal has been shifted of a time interval

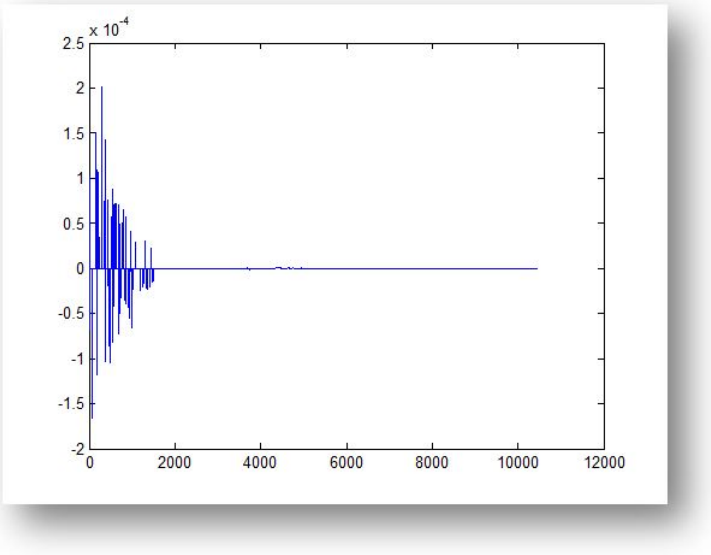

(a)

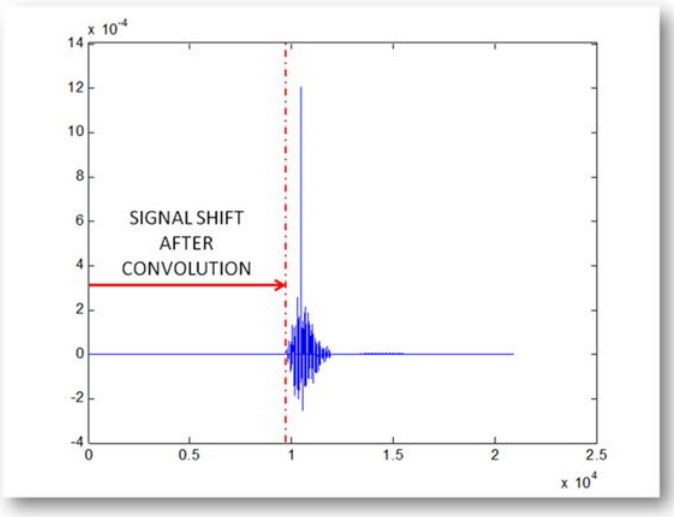

(b)

Fig. 4.3: Traditional multipath channel (a); time shift in the "equivalent TR" channel when transmission pre-filters are used (b).

that is less than a frame duration. The decision on the transmitted bit is soft when a repetition code is used, and in this first study we consider the variable $r_{MUI}[n]$ at the output of the correlator as the sum of the N_s variables associated to the same bit transmitted. As we will see in the following, this makes the MUI distribution more Gaussian with respect to the distribution evaluated on variables associated to single pulses, so pulse-by-pulse distributions are more accurate. We have defined the processing gain as $N = N_s N_h$ and the system load as K/N according to [13]. The study of the distribution of the MUI term has been conducted by varying N_{in}, N_{out}, N_h, N_s, K and keeping the system load fixed to 0.5. The values of (N_{in}, N_{out}) considered are listed in Table 4.1.

Fingers of transmission pre-filter N_{in}	Taps of rake receiver N_{out}
All	1
20	10
20	20
10	20
1	All

Table 4.1: Time Reversal configuration.

For each couple (N_{in}, N_{out}), we have studied the distribution of the variable associated to the MUI signal at the correlator output in each of the cases listed in Table 4.2. Notice that the system load K/N is constant, while processing gain N and the number of users K increase. We have considered IEEE 802.15.3a LOS channels [14]. Moreover, the transmitted sequences of symbols for all users and the relative delays change at each loop. A chip time $T_c = 2$ ns is chosen, the sampling ferquency is $f_c = 50$ GHz, the shift intro-

Case	N_s	N_h	K
1	1	24	12
2	2	48	48
3	4	50	100

Table 4.2: Repetition codes, Cardinality of Time Hopping Code and Number of users.

duced by the PPM has been set to $d_{PPM} = 0.5$ ns, while the values assumed by SNR are [0 3 6 9] dB. At first, our study focuses on the particular case in which the transmission pre-filter consist of all channel paths (reversed in time) and the rake receiver is a one finger rake ($N_{in} = all, N_{out} = 1$). So the equivalent TR channel is the whole $h_{TR}(t) = h(-t) * h(t)$: in this way the complexity is moved from receiver to transmitter (this is one of the most important advantages of TR). The distributions of the correlator output r_{mui}, when in input there is the MUI signal, resulting from simulations conducted in the cases of Table 4.2 are shown in Fig. 4.4, where the MUI histograms and the reference Gaussian distributions with the same variance are represented.

We can notice that the MUI distribution is no more Gaussian when we use the TR technique, but it seems to be more peaked with respect to the reference Gaussian distribution with same variance. The MUI distribution approaches a Gaussian if the processing gain $N = N_s N_h$ and the number of users K grow, because in order to reach the domain of validity of the asymptotic regime in which the SGA can be a valid approximation (at least in the classical scheme without Time Reversal), discussed in 2.3, we have to use a large processing gain and a large number of users [13]. The performance in terms of BER vs. SNR achieved in the three cases are shown in Fig. 4.5. From the analysis of Fig. 4.5, we can see that in this case the introduction

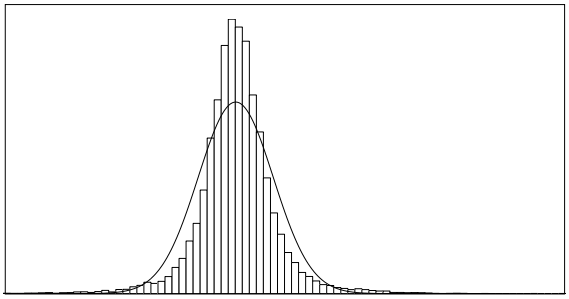

(a) Case 1, Kurtosis = 8.16

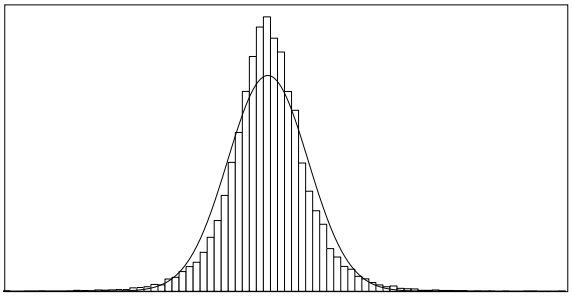

(b) Case 2, Kurtosis = 5.55

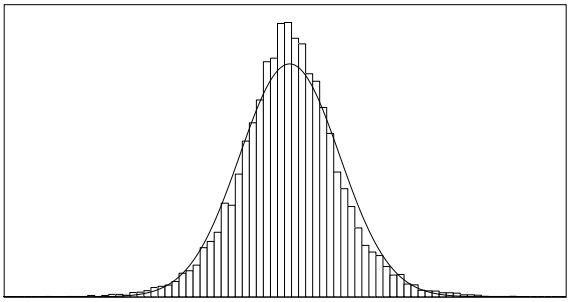

(c) Case 3, Kurtosis = 4.17

Fig. 4.4: MUI histograms and reference Gaussian distributions with same variances for $N_{in} = all$, $N_{out} = 1$. IEEE 802.15.3a LOS channels.

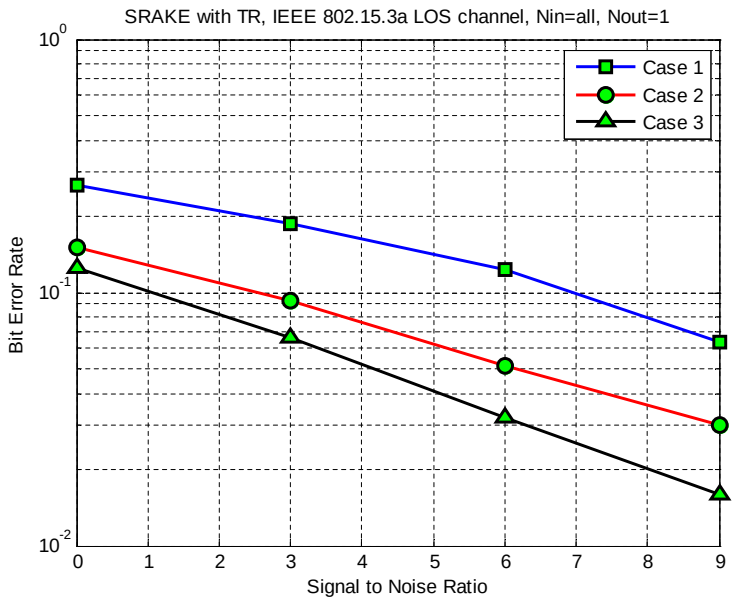

Fig. 4.5: BER vs. SNR for one-finger rake with complete TR ($N_{in} = all$, $N_{out} = 1$).

of a repetition code compensates the effects of a stronger multi-user interference resulting from an higher number of interfering users, so performances are better when N_s grows. We expect that if we reduce the impact of TR by considering a lower number of fingers in the pre-filter, the MUI distribution approaches increasingly a Gaussian. This aspect has been confirmed by simulations: as expected, since the fingers of the transmission pre-filter decrease, the impact of TR is less significant and the kurtosis of the distribution is closer to 3, the value of the kurtosis of a Standard Gausssian distribution. In order to show this we have used a partial pre-filter at the transmitter, with $h_{in}(t)$ being composed of the 20 best paths of $h(-t)$, and a Selective Rake receiver with 10 fingers. The resulting MUI distributions are shown in Fig. 4.6. In this case, distributions approach the reference Gaussians more than in the first case of study, in which we have considered a full TR pre-filter. However,

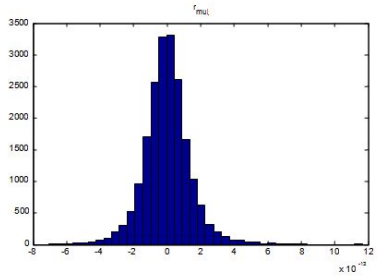

(a) Case 1, Kurtosis = 5.67

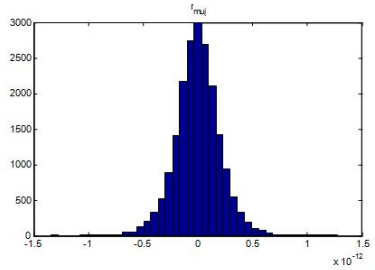

(b) Case 2, Kurtosis = 4.51

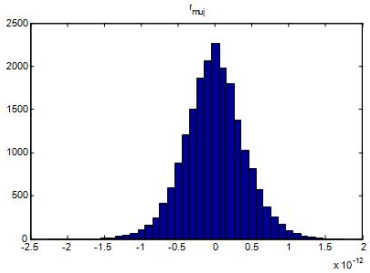

(c) Case 3, Kurtosis = 3.62

Fig. 4.6: MUI histograms and reference Gaussian distributions with same variances for $N_{in} = 20$, $N_{out} = 10$. IEEE 802.15.3a LOS channels.

the kurtosis is still high and this means a "less" Gaussian distribution even in this case in which we have used a less complex TR pre-filter. Other simulations have been carried out for the case in which we have the same number of fingers both in the transmission pre-filter and in Selective Rake receiver. The MUI distributions for the three usual cases in which N_s, N_h and K vary while K/N is kept constant are shown in Fig. 4.7, where N_{in} and N_{out} have been set to 20. As said, we expect that if we reduce the impact of TR by considering a lower number of fingers in the pre-filter, the MUI distribution approaches increasingly a Gaussian. In order to verify this aspect, we have carried out simulations with $N_{in} = 10$ and $N_{out} = 20$ (see Fig. 4.7). As expected, since the fingers of the transmission pre-filter decrease, the impact of TR is less significant and the kurtosis of the distribution is closer to 3. We have carried

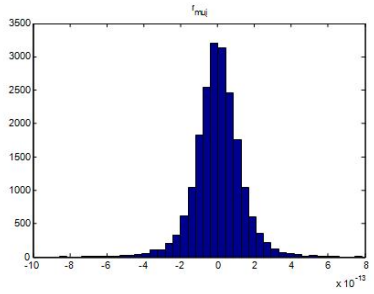

(a) Case 1, Kurtosis = 5.37

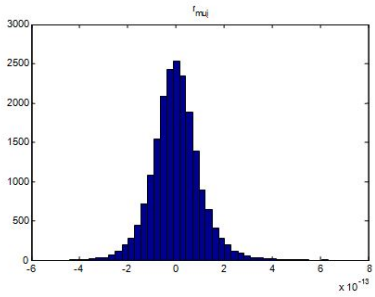

(b) Case 1, Kurtosis = 4.42

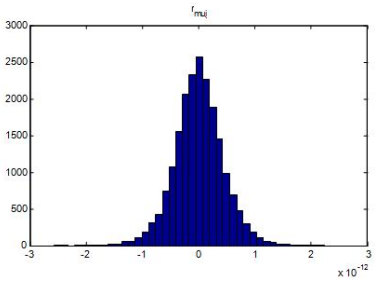

(c) Case 2, Kurtosis = 4.07

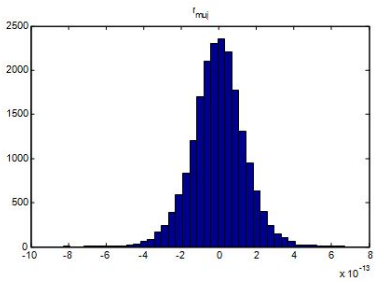

(d) Case 2, Kurtosis = 3.90

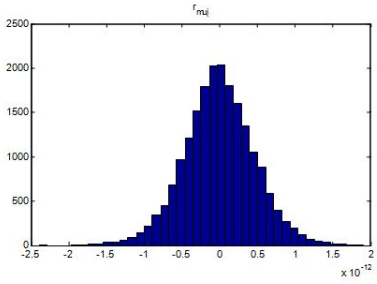

(e) Case 3, Kurtosis = 3.53

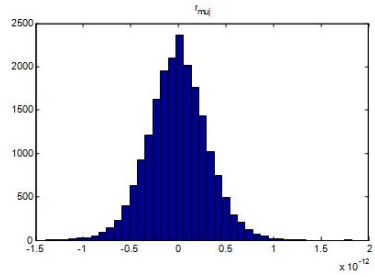

(f) Case 3, Kurtosis = 3.51

Fig. 4.7: MUI histograms and reference Gaussian distributions with same variances for $N_{in} = 20$, $N_{out} = 20$ (left) and $N_{in} = 10$, $N_{out} = 20$ (right). IEEE 802.15.3a LOS channels.

out another simulation in order to return to the condition of absence of TR, so we set Nin to 1 and we have considered an All Rake receiver ($N_{out} = all$). We expect that in this case the MUI distribution could approach a Gaussian one better than in all the previous cases. The results of simulations shown in Fig. 4.8 confirm this aspect: without TR, that is $N_{in} = 1$, and considering an All Rake receiver ($N_{out} = all$), MUI distribution approaches a Gaussian one better than in all the other cases listed in Table 4.1. Because we have

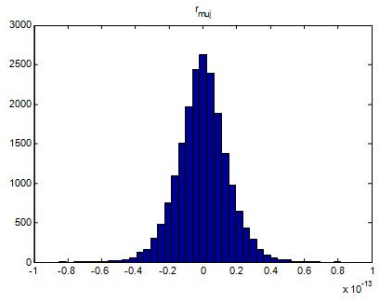

(a) Case 1, Kurtosis = 3.86

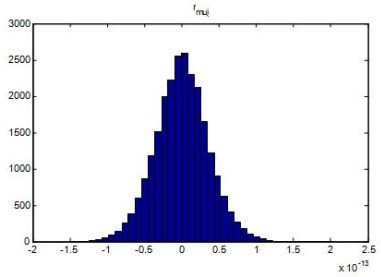

(b) Case 2, Kurtosis = 3.40

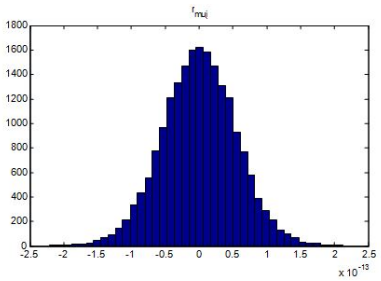

(c) Case 3, Kurtosis = 3.23

Fig. 4.8: MUI histograms and reference Gaussian distributions with same variances for $N_{in} = 1$, $N_{out} = all$. IEEE 802.15.3a LOS channels.

noticed that in our results all expectations are conditioned on the channel of user 1, in the following this channel is kept fixed while the channels of all other users change at each loop. We have verified that the non-Gaussianity of distribution is even more marked in a worst case network topology, in

which the intended transmitter is located at the maximum distance from receiver and the $K = 30$ users are equispaced on the circumference having as diameter this distance. A strong repetition code has been used ($N_s = 6$), the maximum distance from receiver has been set to 10 meters, the symbol interval is $T_s = 96$ ns, the cardinality of Time Hopping code is 48, having kept the chip interval T_c to 2 ns. The power per pulse transmitted by all users, after the TR pre-filters, is the same (-30 dBm), while received power depends on the distance from the receiver. Before evaluating performance, we wait to receive at least 100 wrong bits. The performance in terms of

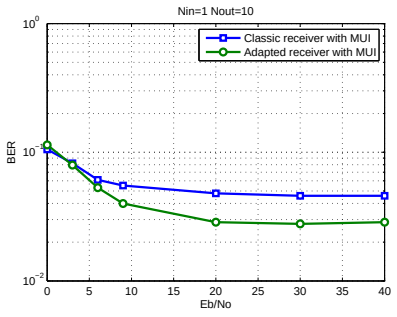

(a) BER vs. SNR with N_{in}=1, N_{out}=10

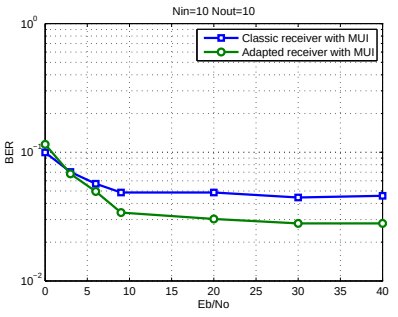

(b) BER vs. SNR with N_{in}=10, N_{out}=10

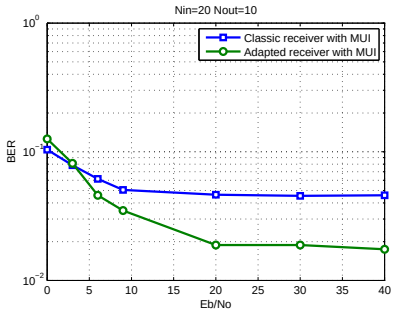

(c) BER vs. SNR with N_{in}=20, N_{out}=10

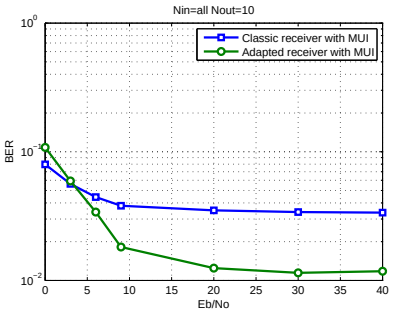

(d) BER vs. SNR with N_{in}=all, N_{out}=10

Fig. 4.9: Performance comparison between classic and adapted receiver with different TR configurations and $N_{out} = 10$.

BER vs. SNR, with $N_{out} = 10$ and varying N_{in}, are shown in Fig. 4.9, while the pulse-by-pulse r_{MUI} distributions are shown in Fig. 4.10. Even in this case increasing the TR impact, the r_{MUI} distribution becomes more tigth (the kurtosis increases, as shown in Fig. 4.10), the difference of performance achieved by the classical receiver and that adapted to a Generalized Gaussian grows, the absolute performance of the adapted receiver increases, while there is not a significant change of classical receiver performance, as we can see in Fig. 4.9. The performance improvement achieved with the receiver

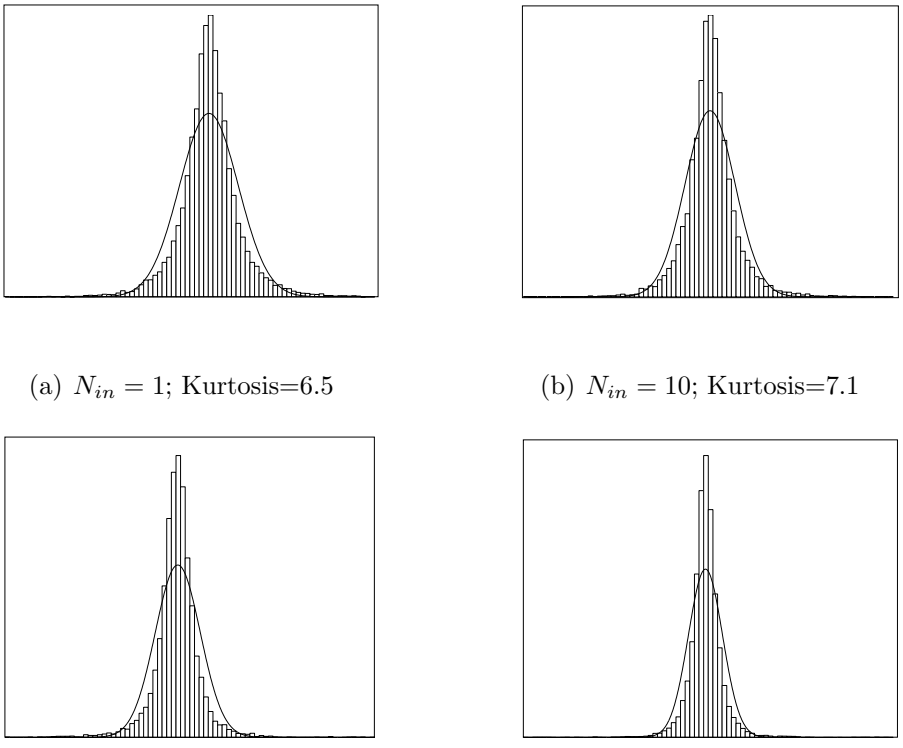

(a) $N_{in} = 1$; Kurtosis=6.5

(b) $N_{in} = 10$; Kurtosis=7.1

(c) $N_{in} = 20$; Kurtosis=12.8

(d) $N_{in} = all$; Kurtosis=20.6

Fig. 4.10: Pulse-by-pulse r_{MUI} distributions with different TR configurations and $N_{out} = 10$.

adapted to a Generalized Gaussian distribution is due to the fact that, as

said, a such distribution better fits the MUI distribution than a Standard Gaussian with the same variance, as we can see in Fig. 4.11.

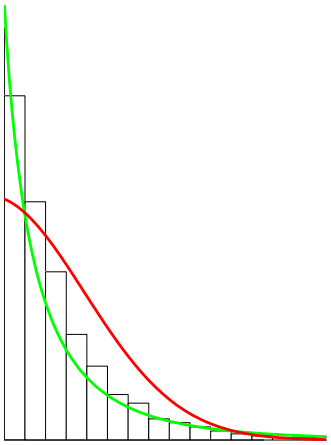

Fig. 4.11: Histogram of r_{MUI} distribution (detail), Standard Gaussian (red) and Generalized Gaussian (green) with same variance. $N_{in} = all$, $N_{out} = 10$

.

Then we focus on the case in which an All Rake receiver has been used, in order to show the improvement of performance achievable in the passage from a scheme without TR, in which a classical receiver is used, to one in which we use a complete TR configuration and both a classical receiver and a receiver adapted to a Generalized Gaussian interference. Simulations results are shown in Fig. 4.12, from the analysis of which we can confirm that using TR we have an improvement of performance both with classical and with adapted receiver. We can note two types of gain brought by TR: the first gain is due to the fact that, as we will see in the following, TR allows to collect more energy at the receiver side. The second gain that we exhibit here is due to the change of MUI distribution which becomes

more far from a Gaussian. The first gain (increasing received energy) gives a low performance improvement because the interfering users use also TR and so the interference also has an increasing energy. This small performance improvement is shown in Fig. 4.12 in the difference of performance between the two classical receivers. The second gain that we exhibit (due to the MUI distribution change) is stronger. It can be noticed in the performance curves obtained with the receivers adapted to the MUI distribution (Fig. 4.12).

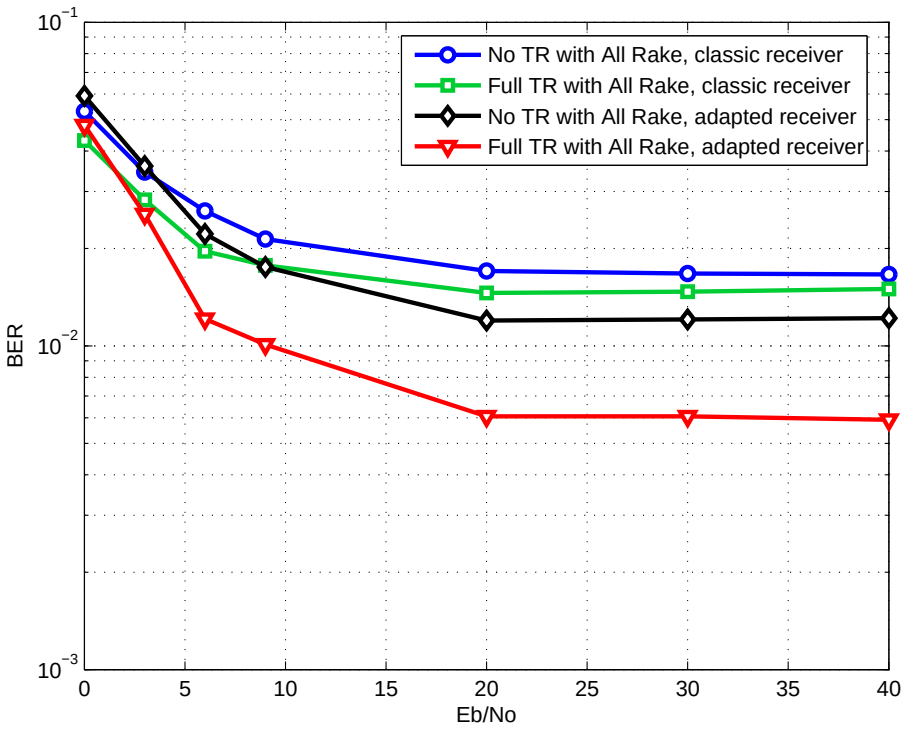

Fig. 4.12: BER vs. SNR with classic and adapted receiver in the cases of TR absence and full TR configuration

From the comparison between the performance curve of the classical receiver in a traditional UWB system and that of the adapted receiver in a Full-TR system (Fig. 4.12), we can notice a big improvement in terms of

BER vs. E_b/N_0 that makes Time Reversal suitable to be used in UWB-IR systems in combination with receivers adapted to a Generalized Gaussian distribution.

In Fig. 4.13 we underline that pulse-by-pulse statistics are more accurated than the same ones obtained by summing up the N_s variables corresponding to the pulses representing the same information bit.

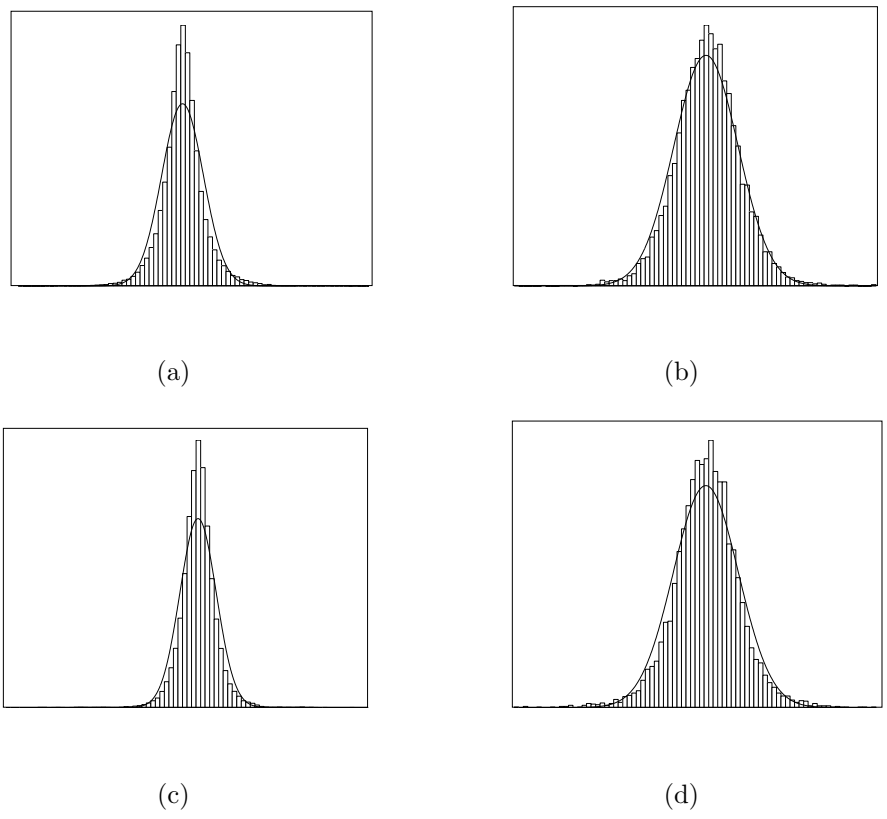

Fig. 4.13: Pulse-by-pulse r_{MUI} distributions (left) and same distributions evaluated over N_s consecutive pulses (right) for $N_{in} = 1, N_{out} = all$ (a), (b) and $N_{in} = all, N_{out} = all$ (c), (d).

As said, the SGA in a system that makes use of TR techinque is less accurate with respect to the traditional non-TR scheme, leading to a too optimistic estimate of classical correlation receiver performance. Simulations

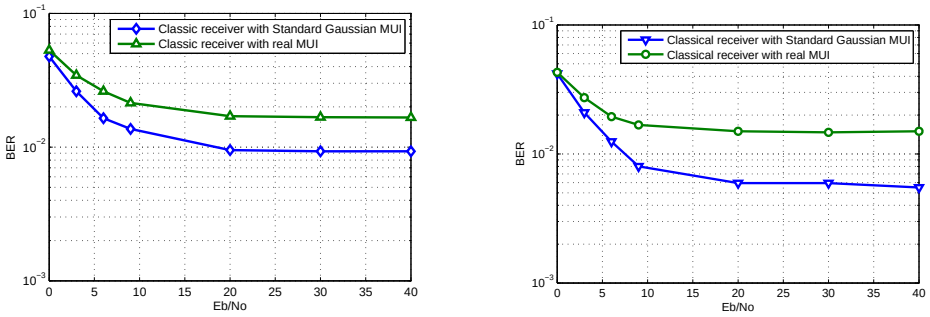

(a) (b)

Fig. 4.14: Non-validity of SGA approximation. Tradional All Rake receiver without TR (a). All Rake receiver combined with TR, $N_{in} = 20$ (b).

confirm this aspect, as underlined in Fig. 4.14, that shows the gap of performance that occurs if a realistic MUI and a Standard Gaussian one with same variance arrive at the classical receiver, in the two cases of absence of TR and its use. Moreover, it is remarkable that the received power per pulse grows not only with N_{out}, keeping fixed the number of TR pre-filter fingers N_{in}, but even with N_{in}, keeping fixed N_{out}, as shown in Table 4.3.

	$N_{in} = 1$	$N_{in} = 10$	$N_{in} = 20$	$N_{in} = all$
$N_{out} = 1$	0.15η	0.54η	0.75η	0.99η
$N_{out} = 10$	0.55η	0.82η	0.98η	1.20η
$N_{out} = 20$	0.75η	0.94η	1.12η	1.32η
$N_{out} = all$	η	1.42η	1.65η	1.92η

Table 4.3: Received powers per pulse

This is due to the focusing properties of Time Reversal, that condenses more and more energy on the main path of the channel if N_{in} increases, as shown in Fig. 4.15. In fact, the temporal focusing introduced by TR makes the receiver able to collect more energy with respect to the case in with

transmission pre-filters are absent, the transmitted power being equal. This is the reason why we can obtain a performance enhancement using Time Reversal also with a classical rake receiver.

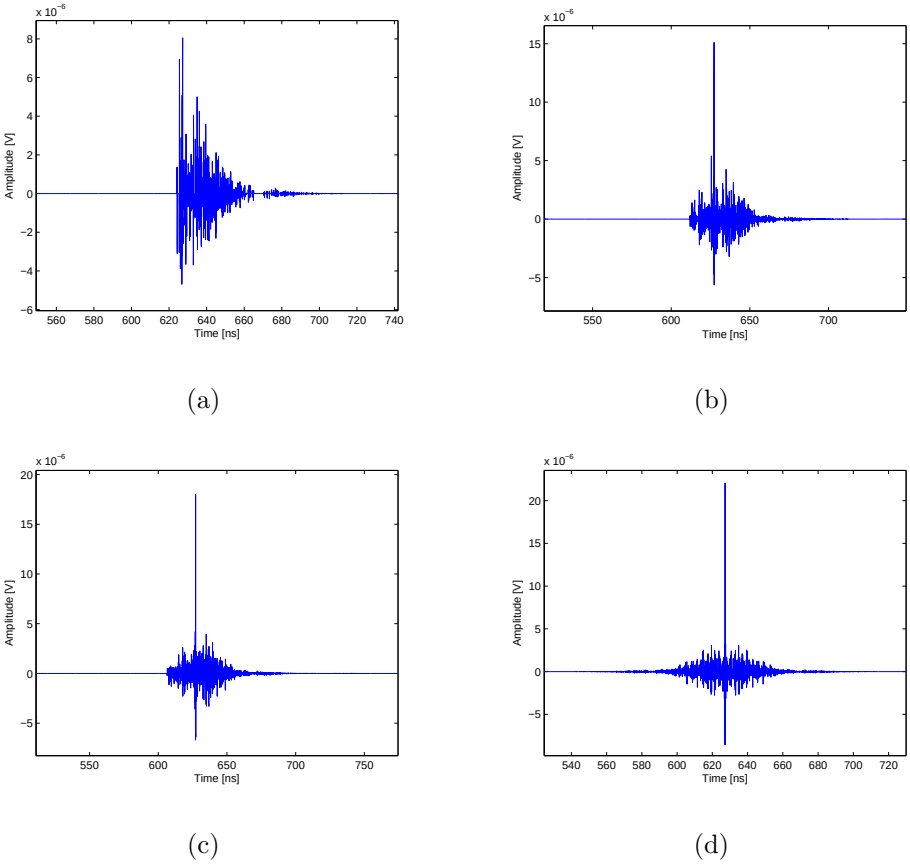

Fig. 4.15: Examples of received pulses with $N_{in} = 1$ (a), $N_{in} = 10$ (b), $N_{in} = 20$ (c), $N_{in} = all$ (d).

Finally, we consider another case study in which we return to a star topology, but this time we have dominant interferers that transmit 10 dB above the useful signal. System parameters are: $T_s = 120$ ns, $N_h = 60$, $N_s = 4$, $N_{in} =$ all, $N_{out} = 1$, P_{tx} per pulse = -30 dBm, $P_{tx_{int}}$ per pulse = -20 dBm, $K = 30$, Distance from rx = 10 m. In Fig. 4.16(a) the performance achievable with classical and adapted receiver are shown. The pulse-by-

pulse distribution of r_{MUI} is shown in Fig. 4.16(b): we can notice that even in this case it is definitely more tigth than a Standard Gaussian, being the kurtosis 6.9. As said, this change in MUI distribution allows to reach better performance using the adapted receiver, even in the cases in which we have strong interferers.

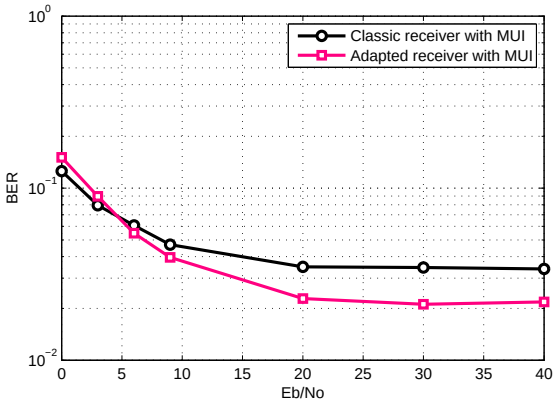

(a)

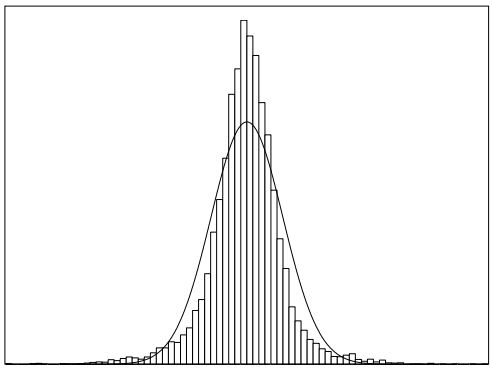

(b)

Fig. 4.16: Performance in terms of BER vs. SNR in a star topology with TR and dominant interferers (a). Pulse-by-pulse r_{MUI} distribution (b).

Chapter 5

Conclusions

In this work we have shown that Time Reversal, applied to Ultra Wide Band - Impulse Radio systems, has an impact on the distribution of multi-user interference, that has been studied in several reference scenarios with multipath channels, varying the transmission parameters (number of users, power trasmitted by intended and interfering transmitters, repetition code) in various network topologies. We have underlined the limits of validity of Standard Gaussian Approximation for the MUI distribution and that the use of Time Reversal, in a UWB-IR communication system affected by multi-user interference, leads to improved performance both with a classical rake receiver and with a receiver adapted to a Generalized Gaussian distribution, that better fits MUI distribution in UWB-IR- TR systems. The study has been performed in several cases in which the TR technique has been used in a more or less deep way. The main results obtained in this work can be summarized as follows.

Time Reversal modifies the multi-user interference distribution, that becomes decreasingly Gaussian with respect to a traditional system, if the number of fingers of transmission pre-filter grows. The SGA, that is too

optimistic even in traditional cases, results still less accurate in a UWB-IR system that implements the Time Reversal technique and this is advantageous because it is known that the Gaussian intereference gives worst channel capacity. Therefore, in these systems we can improve performance using a receiver adapted to a Generalized Gaussian distribution even with strong interferers and particularly unfavourable network topologies. The second result brought by our work consists in the fact that using TR we can have a performance improvement also with a classical receiver, because the received energies increase with respect to the traditional case. This gain gives a low performance improvement because the interfering users use also TR and so the interference also has an increasing energy.

Bibliography

[1] Abiodun E. Akogun, Robert C.Qiu, and Nan Guo. "Demonstrating Time Reversal in Ultra-wideband Communications Using Time Domain Measurements". 51st International Instrumentation Symposium, 8-12 May 2005, Knoxville, Tennessee.

[2] A. Derode, P. Roux, and M. Fink. Robust acoustic time reversal with high-order multiple scattering. In *Phys. Rev. Letters*, volume 75. 1995.

[3] A. Derode, A. Tourin, and M. Fink. In *J. Appl. Phys.*, volume 85, pages 6343–6352. 1999.

[4] M.G. Di Benedetto and G. Gianicola. *Understanding Ultra Wide Band Radio Fundamentals.* Prentice Hall Pearson Education Inc., Upper Saddle River, New Jersey, 2004.

[5] G. Durisi and G. Romano. "On the Validity of Gaussian Approximation to Characterize the Multiuser Capacity of UWB TH-PPM". In *IEEE Conf. on Ultra Wideband Systems and Technologies*, 2002.

[6] S.M. Emami, J. Hansen, A.D. Kim, G. Papanicolau, A.J. Paulraj, D. Cheung, and C. Prettie. "Predicted Time Reversal Performance in Wireless Communications Using Channel Measurements". In *IEEE Comm. Lett.* 2004.

[7] M. Fink and C. Prada. Acoustic time-reversal mirrors. In *Inverse Problems 17*, pages R1–R38. Institue of Physics publishing, 2001.

[8] Mathias Fink. Time Reversal of Ultrasonic Fields - Part I: Basic Principles. In *IEEE transactions on ultrasonics, ferroelectrics and frequency control*, volume 39, September 1992.

[9] Mathias Fink. Time-reversal waves and super resolution. In *4th AIP International Conference and the 1st Congress of the IPIA, Journal of Physics: Conference Series 124*, (2008) 012004.

[10] J. Fiorina and D. Domenicali. "Revisiting TH-IR-UWB performance limits dependency on essential system parameters using the Generalized Gaussian Approximation". In *ICUWB*, September 24-26 2007.

[11] J. Fiorina and W. Hachem. "Central Limit Results for the Multiple User Interference at the SUMF Output for UWB Signals". In *International Symposium on Information Theory and its Applications, ISITA2004*, Parma, Italy, October 10-13 2004.

[12] J. Fiorina and W. Hachem. "Elaboration of a simple receiver adapted to Multi-User Interferences in Impulse Radio Ultra Wide Band". In *IEEE Globecom 2006*, San Francisco, 27 November-1 December 2006.

[13] J. Fiorina and W. Hachem. "On the Asymptotic Distribution of the Correlation Receiver Output for Time-Hopped UWB Signals". In *IEEE Transactions on Signal Processing*, July 2006.

[14] J. Foerster. *Channel modeling Sub-Committee Report Final.* IEEE P802.15-02/490rl-SG3a, February 2003.

[15] X. Liu, B.-Z. Wang, S. Xiao, and J. Deng. Performance of Impulse Radio UWB Communications based on Time Reversal technique. In *Progress In Electromagnetics Research, PIER 79*, pages 401–413, Chengdu 610054, China, 2008. Institute of Applied Physics University of Electronic Science and Technology of China.

[16] H. Niu, J.A. Ritcey, and H. Liu. "Performance of UWB RAKE Receivers with Imperfect Tap Weights". In *IEEE ICASSP*, volume 4, pages 125–128, April 2003.

[17] D. Panaitopol, J. Fiorina, and M.G. Di Benedetto. "Trade-off Between the Number of Fingers in the Prefilter and in the Rake Receiver in Time Reversal IR-UWB". In *ICUWB*, September 9-11 2009.

[18] M.A. Rahman, S. Sasaki, J. Zhou, S. Muramatsu, and H. Kikuchi. "Evaluation of Selective Rake Receiver in Direct Sequence Ultra Wideband Communications in the Presence of Interference ". In *Joint UWBST IWUWBS, 2004 International Workshop*, pages 221–225, May 2004.

[19] P. Roux and M. Fink. *J. Acoust. Soc. Am.*, 107:2418–2429, 2000.

[20] P. Roux, B. Roman, and M. Fink. In *Appl Phys Lett*, volume 70, pages 1811–1813.

[21] T. Strohmer, M. Emami, J. Hansen, G. Papanicolaou, and A.J. Paulraj. "Application of time-reversal with MMSE equalizer to UWB communications". In *Proceedings of IEEE Global Telecommunications Conference (GLOBECOM '04)*, volume 5, pages 3123–3127. Dallas, Tex, USA, November-December 2004.

[22] R. Tombaugh and S. Vasana. "A RAKE Receiver Employing Maximal Ratio Combining (MRC) Without Channel Estimation for UWB Communications". *Osprey Journal*, 2007.

Appendix A

MATLAB codes

```
clear;
clc;
warning off;
close all;

%=========== UWB TRANSMISSION PARAMETERS ================================%
fprintf('Getting transmission parameters\n\n');

Ns=input('Ns = 4 or 6?');   %repetition code;
    if Ns==4                %number of bits transmitted in each loop
        numbits=300;
    elseif Ns==6
        numbits=200;
    end

fprintf('%g bits (%g pulses) transmitted at each loop\n',...
        numbits, Ns*numbits);
Nu=input('Number of active transmitters = ');

l=0;
Ts=96e-9;               %=Nh.*Tc; pulse interval
Tc=2e-9;                %chiptime
fc=50e9;                %sampling frequency
Nh=(Ts/Tc);             %cardinality of TH code
```

```
dPPM=0.5e-9;            %time shift introduced by the PPM [s]
numpulses=Ns*numbits;   %number of pulses per bit

exno=[0 3 6 9 20 30 40];%values assumed by SNR

WB=zeros(1,length(exno));%inizialization of wrong bits vector
accbits=0;              %bits counter

Nin=input('Number of TR pre-filter fingers Nin? (0=all) ');
Nout=input('Number of rake receiver fingers Nout? (0=all) ');
Pow=input('Power to transmit (dBm)?');
Pow_int=input('Power transmitted by interfering users (dBm)?');

tx=1;                   %used later in TMG evaluation
Tm = 0.5e-9;            %pulse duration
tau = 0.2e-9;           %shape factor
%=========================================================================%


%=============== TOPOLOGY ================================================%
topology=input('Topology?\n1=Star\n2=Worst case\n');

LOS=1;
if LOS==1
    A0=47;
    gamm=1.7;
else
    A0=51;
    gamm=3.5;
end
c0=10^(-A0/20);

%Star topology
if topology==1
    distance=10;

%Worst case topology
elseif topology==2
    maxDistance=10;
    [distances_int] = WorstCaseTopology(Nu,maxDistance);
end
```

```
%=========================================================================%

%=========== LOADING REFERENCE IEEE 802.15.3a LOS CHANNEL ================%
load channelLOS2;
l0=length(HF_ref);
clear h0 OT ts X TMG;
H0=zeros(Nu-1,l0);
HF=zeros(Nu-1,l0);
OT=zeros(1,Nu-1);
ts=zeros(1,Nu-1);
X=zeros(1,Nu-1);
%=========================================================================%


%============= IMPULSE RESPONSE INVERSION AND TR APPLICATION =============%
fprintf('Impulse responses inversion and Time Reversal pre-filter for the
      intended user\n');
H_in_ref=fliplr(HF_ref); %Reversing channel

%Transmission pre-filter of reference user
if Nin~=0
    H_in_ref= best_selector(H_in_ref,Nin);
end

%TR channel
TR_CH_ref=fconv(H_in_ref,HF_ref);

if Nout==0 %Case Nout=all
   H_out_ref=TR_CH_ref;
else
   H_out_ref = best_selector(TR_CH_ref,Nout);
end
%=========================================================================%


%============================ LOOPS ======================================%
%At each loop, "numbits" bits are transmitted and new channels for the
%interfering users are generated.
a=0;
while WB(length(exno))<100
```

```
        l=l+1;
        clear TR_CH Smui rx mask_TR;
    fprintf('\nAttempt %g\n',l);
    fprintf('Loading IEEE 802.15.3a channels and impulse response inversion for
          interfering users\n');

    for i=1:(Nu-1)

        %Channel generation for interfering users
        if topology==1
            [rx,ag]=CP0801_PATHLOSS(tx,c0,distance,gamm);
        elseif topology==2
            [rx,ag]=CP0801_PATHLOSS(tx,c0,distances_int(i),gamm);
        end
        TMG(i)=ag^2;
        [H0(i,:),HF(i,:),OT(i),ts(i),X(i)] = cp0802_IEEEuwbMOD(fc,TMG(i),l0);
        H_in(i,:)=fliplr(HF(i,:));

        %Transmission pre-filters of interfering users
        if Nin~=0
            H_in(i,:)= best_selector(H_in(i,:),Nin);
        end

        %TR channel of interfering users
        TR_CH(i,:)=fconv(H_in(i,:),HF(i,:)); %fast convolution

    end
    clear rx ag TMG OT H0 ts X;
    %=========================================================================%


    %=========================================================================%
    fprintf('2PPM-TH-UWB signals generation\n');
    for i=1:Nu
        %2PPM-UWB signal generation
        [bits(i,:),THcode(i,:),Stx,ref]=CP0201_TRANSMITTER_2PPM_TH_TR1(Ns,
              numbits,Ts,Tc,dPPM);
        [pulse,Ex]=ONE_PULSE_TRANSMITTER(Ts);

        if i==1 %Reference transmitter
```

```
145         %Energy evaluation after TR pre-filter
            pulse_prefilter_out=fconv(pulse,H_in_ref);
            en_ppo_ref=sum(abs(pulse_prefilter_out).^2.*(1/fc));

            %Energy normalization
150         power = (10^(Pow/10))/1000;
            E_Stx_ref = power * Ts;
            Stx_ref1=Stx;
            Stx_ref=Stx.*sqrt(E_Stx_ref)/sqrt(en_ppo_ref);

155         fprintf('Through the channel %g/%g...\n',i,Nu);
            Srx_temp=fconv(Stx_ref,TR_CH_ref);
            Srx_ref=Srx_temp(1:length(Stx_ref));
            Smui=zeros(1,length(Srx_ref));
            ref_ref=ref;
160

        else %interfering users

            %Energy evaluation after TR pre-filter
165         pulse_prefilter_out=fconv(pulse,H_in((i-1),:));
            en_ppo=sum(abs(pulse_prefilter_out).^2.*(1/fc));

            %Energy normalization
            power = (10^(Pow_int/10))/1000;
170         E_Stx = power * Ts;
            Stx=Stx.*sqrt(E_Stx)/sqrt(en_ppo);

             %Asynchronism introduction
             [Stx] = Async_user(Stx,fc,Ts);
175          fprintf('Through the channel %g/%g...\n',i,Nu);
             Srx_temp=fconv(Stx,TR_CH((i-1),:));
             acc=Srx_temp(1:length(Stx));
             Smui=Smui+acc;
        end
180 end
    clear Srx_temp acc  ref H_in S_tx;
    %=========================================================================%


185 %==================== ADDING NOISE ===============================================%
```

```
fprintf('Adding noise\n');
tx_pulse_ref=pulse.*sqrt(E_Stx_ref)/sqrt(en_ppo_ref);
rx_pulse_ref=fconv(tx_pulse_ref,TR_CH_ref);
en_rx_pulse_ref=sum(abs(rx_pulse_ref).^2);
[output, noise] = cp0801_Gnoise2mod(en_rx_pulse_ref,exno,Srx_ref);
%=========================================================================%


%=================== RECEIVED SIGNAL ====================================%
for i=1:length(exno)
    rx(i,:)=Smui+output(i,:);
end
%=========================================================================%


%============= CORRELATOR ===============================================%
fprintf('Creating correlator mask\n');
mask_TR=cp0803_PPMcorrmask_R_FAST(ref_ref,fc,numpulses,dPPM,H_out_ref);

fprintf('Data acquisition and processing with evaluation of performances\n')
      ;


first_max_rx=find(TR_CH_ref==max(TR_CH_ref));
st=first_max_rx+1;
dt = 1 / fc;                        % sampling time
framesamples = floor(Ts ./ dt);     % number of samples per frame
bitsamples = framesamples * Ns;     % number of samples per bit
pulses_loss=ceil(st/framesamples);
pulses_signif=numpulses-pulses_loss;
numbits_signif=numbits-ceil(pulses_loss/Ns);

[WBacc,mx_shifted] = cp0801_PPMreceiver_TRMOD1(rx,mask_TR,fc,bits(1,:),
      numbits,numbits_signif,Ns,Ts,Stx_ref,TR_CH_ref);
WB=WB+WBacc;
accbits=(numbits_signif-1)+accbits;

[zp1(l,:)] = correlator_output_TR(Smui,mask_TR,fc,numbits,Ns,Ts,Stx_ref,
      TR_CH_ref);
zp(l,:)=zp1(l,(Ns+1):(numbits_signif*Ns));
```

```
[v(l,:)] = correlator_output_TR(Srx_ref,mask_TR,fc,numbits,Ns,Ts,Stx_ref,
      TR_CH_ref);
v1(l,:)=v(l,(Ns+1):(numbits_signif*Ns));

bits_tot_signif(l,:)=bits(1,2:numbits_signif);

for n=1:length(exno)
    [x_imp_temp1(a+n,:)] = correlator_output_TR(rx(n,:),mask_TR,fc,numbits,
          Ns,Ts,Stx_ref,TR_CH_ref);
    x_imp_temp(a+n,:)=x_imp_temp1((a+n),(Ns+1):(numbits_signif*Ns));
    [noise_var_temp1(a+n,:)] = correlator_output_TR(noise(n,:),mask_TR,fc,
          numbits,Ns,Ts,Stx_ref,TR_CH_ref);
    noise_var_temp(a+n,:)=noise_var_temp1(a+n,(Ns+1):(numbits_signif*Ns));
end

clear WBacc numbits_signifacc;
fprintf('Wrong bits = %g\n',WB(length(exno)));
a=a+length(exno);
end %of while WB(length(exno))<100
%=========================================================================%


%=================== PERFORMANCE EVALUATION ============================%
nAttempts=l;
clear l;
for n = 1 : length(exno)
    BER1(n) = WB(n) / (accbits); % average Bit Error Rate
end
clear x_imp_temp1 noise_var_temp1;

%Evaluation of variable r_mui over nAttempts attempts
r_mui=zp';
r_mui=r_mui(:);
r_mui=r_mui';

%Evaluation of kurtosis
kur_r_mui=kurtosis(r_mui);
fprintf('kurtosis r_mui=%g\n',kur_r_mui);

%Generalized Gaussian MUI generation
```

```
esponente=fzero(inline(['(gamma(5/x)*gamma(1/x)/((gamma(3/x))^2))-3-',
      num2str(kur_r_mui-3)]),1);
[wGGjo] = GG_noise(r_mui,esponente);

%Standard Gaussian MUI generation
[SGA_mui] = SGA_approximation(r_mui);

%Merging of intermediate variables
for p=1:length(exno)
    x_imp=x_imp_temp(p,:);
    noise_var=noise_var_temp(p,:);
    for l=1:(nAttempts-1)
            x_imp=[x_imp x_imp_temp((p+l*length(exno)),:)];
            noise_var=[noise_var noise_var_temp((p+l*length(exno)),:)];
    end
    nuovo(p,:)=x_imp;
    nuovo1(p,:)=noise_var;
    clear x_imp noise_var;
end

x_imp=nuovo;
noise_var=nuovo1;
clear nuovo nuovo1;

ai=v1';
ai=ai(:);
v=ai';
epsilon_su_Ns=abs(v);

bi=bits_tot_signif';
bi=bi(:);
bits_cum=bi';

%Classical and adapted receiver
for n=1:length(exno)

    h_lim(n,:)=(abs(x_imp(n,:)+epsilon_su_Ns).^esponente)-(abs(x_imp(n,:)-
          epsilon_su_Ns).^esponente);

    x_imp2(n,:)=noise_var(n,:)+v+wGGjo;
```

```
h_lim_GG(n,:)=(abs(x_imp2(n,:)+epsilon_su_Ns).^esponente)-(abs(x_imp2(n
      ,:)-epsilon_su_Ns).^esponente);

x_imp3(n,:)=noise_var(n,:)+v+SGA_mui;
h_lim_SGA(n,:)=(abs(x_imp3(n,:)+epsilon_su_Ns).^esponente)-(abs(x_imp3(n
      ,:)-epsilon_su_Ns).^esponente);

t=1;
for m=1:length(bits_cum)
    %outc(n,m)=sum(x_imp(n,t:(t+Ns-1)));    %Classical rx with real MUI
    %RXbitsc(n,m)=(-outc(n,m))>0;
    outa(n,m)=sum(h_lim(n,t:(t+Ns-1)));       %Adapted rx with real MUI
    RXbitsa(n,m)=(-outa(n,m))>0;

    outGGc(n,m)=sum(x_imp2(n,t:(t+Ns-1)));    %Classical rx with GG MUI
    RXbitsGGc(n,m)=(-outGGc(n,m))>0;
    outGGa(n,m)=sum(h_lim_GG(n,t:(t+Ns-1)));    %Adapted rx with GG MUI
    RXbitsGGa(n,m)=(-outGGa(n,m))>0;

    outSGAc(n,m)=sum(x_imp3(n,t:(t+Ns-1)));   %Classical rx with SG MUI
    RXbitsSGAc(n,m)=(-outSGAc(n,m))>0;
    outSGAa(n,m)=sum(h_lim_SGA(n,t:(t+Ns-1)));  %Adapted rx with SG MUI
    RXbitsSGAa(n,m)=(-outSGAa(n,m))>0;

    t=t+Ns;
end

%WBc(n) =  sum(abs(bits_cum(1,:)-RXbitsc(n,:)));
%BERc(n) = WBc(n)/length(bits_cum);
WBa(n) =  sum(abs(bits_cum(1,:)-RXbitsa(n,:)));
BERa(n) = WBa(n)/length(bits_cum);

WBGGc(n) =  sum(abs(bits_cum(1,:)-RXbitsGGc(n,:)));
BERGGc(n) = WBGGc(n)/length(bits_cum);
WBGGa(n) =  sum(abs(bits_cum(1,:)-RXbitsGGa(n,:)));
BERGGa(n) = WBGGa(n)/length(bits_cum);

WBSGAc(n) =  sum(abs(bits_cum(1,:)-RXbitsSGAc(n,:)));
BERSGAc(n) = WBSGAc(n)/length(bits_cum);
WBSGAa(n) =  sum(abs(bits_cum(1,:)-RXbitsSGAa(n,:)));
BERSGAa(n) = WBSGAa(n)/length(bits_cum);
```

```
end
clear noise output rx;
%=========================================================================%

%============================ GRAPHICS ===================================%
figure
semilogy(exno,BER1,exno,BERa);
legend('Classical receiver with real MUI','Receiver adapted to GG with real
      MUI');
xlabel('Eb/No');
ylabel('BER');

figure
semilogy(exno,BERGGc,exno,BERGGa);
legend('Classical receiver with Generalized Gaussian MUI','Adapted receiver
      with Generalized Gaussian MUI');
xlabel('Eb/No');
ylabel('BER');

figure
semilogy(exno,BERSGAc,exno,BERSGAa);
legend('Classical receiver with Standard Gaussian MUI','Receiver adapted to
      GG with Standard Gaussian MUI');
xlabel('Eb/No');
ylabel('BER');

figure
semilogy(exno,BERSGAc,exno,BER1);
legend('Classical receiver with Standard Gaussian MUI','Classical receiver
      with real MUI');
xlabel('Eb/No');
ylabel('BER');

figure;
hist(r_mui,120)
title('r_m_u_i');
%=========================================================================%
```

```
%=========================================================================%
function [distances_int] = WorstCaseTopology(Nu,maxdistance)

a=floor(Nu/2);
for l=1:a
        arco(l)=pi*maxdistance*l/(Nu+1);
        alpha(l)=360*arco(l)/(pi*maxdistance);
        corda(l)=maxdistance*sin(pi*alpha(l)/360);
        distance(l)=sqrt(maxdistance^2-corda(l)^2);

end

distance2=fliplr(distance);
distances_int=[distance distance2];
distances_int=sort(distances_int);
distances_int=distances_int(1:(Nu-1));
%=========================================================================%


%=========================================================================%
function [X_SEL] = best_selector(X,S)
Xord=abs(X);
Xsort=sort(Xord,'descend');
vec_min=Xsort(S);
for i=1:length(X)
    if Xord(i)>=vec_min
        X_SEL(i)=X(i);
    else
        X_SEL(i)=0;
    end
end
%=========================================================================%


%=========================================================================%
function [pulse,Ex]=ONE_PULSE_TRANSMITTER(Ts)

Pow=-30;
power = (10^(Pow/10))/1000;
fc = 50e9;
```

```
tau = 0.2e-9;
Tm = 0.5e-9;
Ex = power * Ts;                % energy per pulse
w0 = CP0201_WAVEFORM(fc,Tm,tau);% Energy Normalized pulse
                                %  waveform
pulse = w0 .* sqrt(Ex);
%=========================================================================%


%=========================================================================%
function [async_signal] = Async_user(signal,fc,Ts)
dt = 1 / fc;                        % sampling time
framesamples = floor(Ts ./ dt);
%Random delay introduction, less than a frame duration
delay=round(rand*framesamples/2);
trail=zeros(1,delay);
async_signal=[trail signal];
async_signal=async_signal(1:length(signal));
%=========================================================================%


%=========================================================================%
%Returns the output of the correlator
% 'Smui' is the MUI signal
% 'mask' is the waveform of the correlation mask
% 'fc' is the sampling frequency
% 'bits' is the binary stream generated by the source
% 'Ns' is the number of pulses per bit
% 'Ts' is the average pulse repetition period [s]

% The function returns the stream before the
% detection process
function [zp] = correlator_output_TR(Smui,mask,fc,numbits,Ns,Ts,Stx,
      TR_CH_ref)

dt = 1 / fc;                        % sampling time
framesamples = floor(Ts ./ dt);     % number of samples per frame
bitsamples = framesamples * Ns;     % number of samples per bit
mx = Smui .* mask;

%Compensating the shift introduced by TR
```

```
    [mx,st]=allinea_rxMOD(Stx,mx,TR_CH_ref);

count_pulses=0;

    for nb = 1 : numbits


            mxk = mx(1+(nb-1)*bitsamples:bitsamples+...
               (nb-1)*bitsamples);


            for np = 1 : Ns

                count_pulses=count_pulses+1;

                mxkp = mxk(1+(np-1)*framesamples:...
                   framesamples+(np-1)*framesamples);
                zp(count_pulses) = sum(mxkp.*dt);

            end % for np = 1 : Ns


        end % for nb = 1 : numbit
%=========================================================================%


%=========================================================================%
function [rx_sh,st]=allinea_rxMOD(Stx,rx,TR_CH_ref)

b=find(Stx==max(Stx));
first_max_rx=find(TR_CH_ref==max(TR_CH_ref))+b(1);
st=first_max_rx-b(1)+1;
rx_sh=rx(1,st:length(rx));
pad=zeros(1,(length(rx)-length(rx_sh)));
rx_sh=[rx_sh pad];
%=========================================================================%


%=========================================================================%
function [wGGjo] = GG_noise(r_mui,esponente)
```

```
L=length(r_mui);
a=esponente;
%(a) is the power inside the generalized gaussian
%We want to generate the Generalized Gaussian:
if a<1
'methode 1'
wGGjo=(gamrnd(1/a,1,L,1).^(1/a)).*sign(randn(L,1));
end

if a>=1
'methode 2'
U=rand(L,1);
compU=U<(1-1/a);
FU=gamrnd(1,1,L,1);
xU=U.*compU+(1+(FU-1)/a).*(1-compU);
TU=gamrnd(1,1,L,1);
AckU=(TU+FU.*(1-compU)-xU.^a)>=0;
AckU=find(AckU);
%accept X if T+f - X^beta >= 0
wGGjo=xU(AckU).*sign(randn(length(AckU),1));
length(wGGjo);
end

s2=(wGGjo'*wGGjo)/length(wGGjo);

%beta coefficient of Kay is:
betav=(2/a)-1;

%this is for drawing the histogram and the corresponding generalized
%gaussian
% beta is not the beta of kay but used in the formula
beta=((gamma(1/a)/gamma(3/a))^(1/2))*((s2)^(1/2));

figure
[t,tt]=hist(wGGjo,120);
hist(wGGjo,120);
title('WGGn');

lll=length(wGGjo);
ttt=tt(2)-tt(1);
hold on
```

```
%ezplot( [ num2str(lll) ,'*', num2str(ttt) ,'*(', num2str(a) ,'/(2*',
      num2str(beta) ,'*gamma(1/', num2str(a) ,')))*exp(-( abs(x)/', num2str(
      beta) ,' )^(', num2str(a) ,') )'])
%end of Drawing

hold off



if length(wGGjo)<length(r_mui)
    for i=length(wGGjo+1):length(r_mui)
        wGGjo(i)=mean(wGGjo);
    end
end

wGGjo=wGGjo/std(wGGjo)*std(r_mui);
wGGjo=wGGjo';
%=========================================================================%



%=========================================================================%
function [SGA_mui] = SGA_approximation(r_mui)
L=length(r_mui);
SGA_mui=randn(1,L);
SGA_mui=SGA_mui/std(SGA_mui)*std(r_mui);
%=========================================================================%
```

- cp0801_pathloss is taken from [4], page 338.
- cp0802_IEEEuwbMOD is a modified version of cp0802_IEEEuwb, taken from [4], pages 352-356.
- CP0201_TRANSMITTER_2PPM_TH_TR1 is a modified version of CP0201_TRANSMITTER_2PPM_TH, taken from [4], pages 58-61.
- cp0801_Gnoise2mod is a modified version of cp0801_Gnoise2, taken from [4], pages 341-342.
- cp0803_PPMcorrmask_R_FAST is a modified version of cp0803_PPMcorrmask_R, taken from [4], pages 363-364. It implements fast convolutions.
- cp0801_PPMreceiver_TRMOD1 is a modified version of cp0801_PPMreceiver, taken from [4], pages 344-347. It takes into account the temporal shift introduced by TR with the insertion of function allinea_rxMOD.